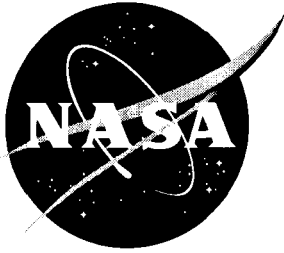NASA/TM-2003-212433

Engine Installation Effects of Four Civil Transport Airplanes: Wallops Flight Facility Study

Gregg G. Fleming
U.S. Department of Transportation
John A. Volpe National Transportation Systems Center, Cambridge, Massachusetts

David A. Senzig
Senzig Engineering, Winchester, Massachusetts

David A. McCurdy
NASA Langley Research Center, Hampton, Virginia

Christopher J. Roof and Amanda S. Rapoza
U.S. Department of Transportation
John A. Volpe National Transportation Systems Center, Cambridge, Massachusetts

October 2003

Since its founding, NASA has been dedicated to the advancement of aeronautics and space science. The NASA Scientific and Technical Information (STI) Program Office plays a key part in helping NASA maintain this important role.

The NASA STI Program Office is operated by Langley Research Center, the lead center for NASA's scientific and technical information. The NASA STI Program Office provides access to the NASA STI Database, the largest collection of aeronautical and space science STI in the world. The Program Office is also NASA's institutional mechanism for disseminating the results of its research and development activities. These results are published by NASA in the NASA STI Report Series, which includes the following report types:

- TECHNICAL PUBLICATION. Reports of completed research or a major significant phase of research that present the results of NASA programs and include extensive data or theoretical analysis. Includes compilations of significant scientific and technical data and information deemed to be of continuing reference value. NASA counterpart of peer-reviewed formal professional papers, but having less stringent limitations on manuscript length and extent of graphic presentations.

- TECHNICAL MEMORANDUM. Scientific and technical findings that are preliminary or of specialized interest, e.g., quick release reports, working papers, and bibliographies that contain minimal annotation. Does not contain extensive analysis.

- CONTRACTOR REPORT. Scientific and technical findings by NASA-sponsored contractors and grantees.

- CONFERENCE PUBLICATION. Collected papers from scientific and technical conferences, symposia, seminars, or other meetings sponsored or co-sponsored by NASA.

- SPECIAL PUBLICATION. Scientific, technical, or historical information from NASA programs, projects, and missions, often concerned with subjects having substantial public interest.

- TECHNICAL TRANSLATION. English-language translations of foreign scientific and technical material pertinent to NASA's mission.

Specialized services that complement the STI Program Office's diverse offerings include creating custom thesauri, building customized databases, organizing and publishing research results ... even providing videos.

For more information about the NASA STI Program Office, see the following:

- Access the NASA STI Program Home Page at *http://www.sti.nasa.gov*

- E-mail your question via the Internet to help@sti.nasa.gov

- Fax your question to the NASA STI Help Desk at (301) 621-0134

- Phone the NASA STI Help Desk at (301) 621-0390

- Write to:
  NASA STI Help Desk
  NASA Center for AeroSpace Information
  7121 Standard Drive
  Hanover, MD 21076-1320

NASA/TM-2003-212433
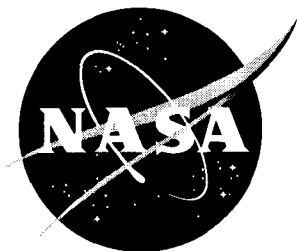
Engine Installation Effects of Four Civil Transport Airplanes: Wallops Flight Facility Study

Gregg G. Fleming
U.S. Department of Transportation
John A. Volpe National Transportation Systems Center, Cambridge, Massachusetts

David A. Senzig
Senzig Engineering, Winchester, Massachusetts

David A. McCurdy
NASA Langley Research Center, Hampton, Virginia

Christopher J. Roof and Amanda S. Rapoza
U.S. Department of Transportation
John A. Volpe National Transportation Systems Center, Cambridge, Massachusetts

National Aeronautics and
Space Administration

Langley Research Center
Hampton, Virginia 23681-2199

October 2003

Available from:

Table of Contents

List of Figures

List of Tables

Executive Summary

This report examines the effects of airplane geometrical configuration on the acoustic directivity characteristics and on the propagation of airplane noise. This effect of airplane geometry is referred to in this report as "engine installation effects." Engine installation effects are one of the components of lateral attenuation. Lateral attenuation in the Federal Aviation Administration's (FAA) Integrated Noise Model (INM) has been based on the methods described in the Society of Automotive Engineers' (SAE) Aerospace Information Report (AIR) 1751. Released in 1981, SAE-AIR-1751 is founded on data measured in the 1960s and 1970s. The Boeing B-727 airplane, which has an engine location not used on more modern large civil transports, dominated these measurements. Long-term measurements conducted with airport noise monitoring equipment have shown that the lateral attenuation algorithms in SAE-AIR-1751 tend to predict too much attenuation for modern airplanes.

The National Aeronautics and Space Administration (NASA), Langley Research Center (LaRC), the Environmental Measurement and Modeling Division of the United States Department of Transportation's John A. Volpe National Transportation Systems Center (Volpe), and several other organizations (see Appendix A for a complete list of participating organizations and individuals) conducted a noise measurement study at NASA's Wallops Flight Facility (Wallops) near Chincoteague, Virginia during September 2000. This test was intended to determine engine installation effects on four civil transport airplanes: a Boeing 767-400, a McDonnell-Douglas DC9, a Dassault Falcon 2000, and a Beechcraft King Air. Wallops was chosen for this study because of the relatively low ambient noise of the site and the degree of control over airplane operating procedures enabled by operating over a runway closed to other uses during the test period. Measurements were conducted using a twenty microphone U-shaped array oriented perpendicular to the flight path; microphones were mounted such that ground effects were minimized and low elevation angles were observed.

The measurements were conducted using equipment capable of producing one-third octave-band noise data and airplane time-space-position information throughout the flight segment of interest. Equipment to perform this task consisted of acoustical instrumentation, meteorological instruments, differential Global Positioning Equipment (dGPS) tracking equipment, video tracking equipment, survey equipment, and other supporting equipment.

The acoustic data recorded at each microphone location were processed into Sound Exposure Levels (SEL) after normalizing to a fixed flight track-to-microphone distance. Differences in normalized sound levels between each microphone and the one directly under the flight is termed the engine installation effect.

The conclusions of the study can be summarized as follows:

*   Airplanes with wing- and tail-mounted engines have substantially different engine installation effects.

*   Departure and arrival airplane configurations (i.e., flap, slat, and thrust settings for these different flight regimes) do not produce substantially different engine installation effects.

*   Lateral attenuation / installation effects for the airplanes with tail-mounted engines measured during this test substantially agree with the SAE-AIR-1751 method.

*   Significant differences exist between airplanes with wing-mounted engines measured during this test and SAE-AIR-1751.

*   Propeller-driven airplanes do not exhibit engine installation effects. It is recommended engine-installation effects not be applied to noise modeling of propeller-driven airplanes.

It is recommended that a modification to SAE-AIR-1751 include the separation of the engine installation component of lateral attenuation into wing-mounted engine installation effects and tail-mounted engine installation effects.

1 Introduction

"Lateral attenuation" refers to the decrease in sound level observed at low elevation angles relative to levels observed directly under an aircraft and at the same slant distance from the receiver to the airplane. Lateral attenuation encompasses many aspects of sound generation and propagation, including ground effects (also referred to as excess ground attenuation), as well as engine installation effects, consisting of shielding and reflections from airplane structures, aerodynamic refraction of sound, and jet shielding due to closely spaced jet engine exhausts. Accurate prediction of lateral attenuation is an essential component in the accurate prediction of airplane noise. Although much work has been done to quantify lateral attenuation as it relates to airplanes[1-5], there continue to be discrepancies between predicted and measured noise levels, especially for situations involving sideline receptors and airplanes at low altitudes, where lateral attenuation effects can be substantial[6,7]. One potential explanation for these discrepancies is the use of older airplanes in the derivation of the lateral attenuation prediction algorithm. This study measures the engine installation effects of both older and more modern airplanes, and suggests modifications to the existing lateral attenuation algorithms in common use.

1.1 Background

The lateral attenuation algorithm in the Society of Automotive Engineers' Airspace Information Report number 1751 (SAE-AIR-1751)[1], and by default most aircraft noise models worldwide, including the FAA's Integrated Noise Model (INM)[8], is based on two separate regression equations. One equation computes ground-to-ground propagation, the other computes air-to-ground propagation. These equations were developed from measured data for 1960s and 1970s airplanes with turbofan engines mounted on the rear fuselage of the airplanes ("tail-mounted"). In SAE-AIR-1751 these equations are presumed applicable to the entire fleet of airplanes, including the more modern types with turbofan engines mounted under the wings ("wing-mounted").

At the most fundamental level, the lateral attenuation of airplane noise comprises two basic physical phenomena, ground effects and engine installation effects. Ground effects, which are fairly well understood, account for the introduction of an impedance boundary, in this case the ground surface, into a given airplane-to-receiver geometry. The general understanding of this phenomenon is based on an assemblage of acoustic research, which includes the work of Ingard[9] in the 1950s, and the later works of Delany and Bazley[10], and Chessell[11]. Engine installation effects account for sound reflections from the airplane wings and fuselage, sound shielding primarily due to the fuselage and any interaction between the airplane-generated sound and the flow field associated with the jet engine exhaust and wing vortices.

1.2 Study Objectives

The current study is a continuation of work begun several years ago to examine the validity of SAE-AIR-1751. This work has been undertaken by organizations in several different countries[6,7]. As part of this on-going work, this study's objectives can be defined as:

- Identify the airplane and engine parameters that affect lateral attenuation.
- Develop recommendations for updating SAE-AIR-1751.

1.3 Airplane Selection

A DC9 was rented from a major airline to match the tail-mounted large civil transports used in the development of SAE-AIR-1751. Honeywell International Inc. donated the use of their Dassault Falcon 2000, a tail-mounted engine airplane with modern high by-pass-ratio (BPR) engines. This airplane was used to determine if the observed engine installation effects in SAE-AIR-1751 were due to the installation of low BPR engines in most tail-mounted engine airplanes. Delta Air Lines provided a 767-400 as an example of a modern high BPR wing-mounted engine airplane. Finally, NASA arranged for the use of its Beechcraft King Air to provide a propeller-driven airplane for the test. These airplanes, with their engines and maximum take-off weights, are presented below in Table 1.

Table 1. Airplanes used in test

Airplane	Description	Engines	Maximum Take-off weights
King Air	Two wing-mounted tractor propellers	PT6A	12,500 lb
Falcon 2000	Two fuselage mounted High Bypass Turbofans	CFE 738	36,000 lb
DC9	Two fuselage mounted Low Bypass Turbofans	JT8D	121,000 lb
767-400	Two wing mounted High Bypass Turbofans	CF6-80	450,000 lb

1.4   Site Selection

In 2000, Volpe and NASA initiated the process of identifying the most suitable locations at which to conduct measurements. Wallops was chosen as the best site meeting the following criteria:

- Relatively low ambient noise.
- Ability to control access to the test site.
- Relatively flat terrain.
- Close proximity to NASA's acoustic equipment in Hampton, Virginia

Relatively low ambient noise was required to improve the signal-to-noise ratio for the test. In this study, the A-weighted Sound exposure Level (SEL) was the metric used. SEL integrates the received signal over a period of time; during this integration time, the signal should remain free of extraneous noise. The Wallops facility is remote from industrial and residential noise sources and met the low ambient noise requirement.

Ability to control access to the test site meant that the test could be conducted on a runway closed to other airport traffic. Although Wallops remained open to other traffic during the test, this traffic was directed to use Wallops' other runway. Closing the test runway also allowed part of the microphone array to be physically placed on the runway.

Relatively flat terrain provided a direct acoustic path from the airplanes to the microphones with no differences between the right and left side of the array. The flat terrain of Wallops also allowed the use of video tracking of the airplanes not equipped with a differential Global Positioning System (dGPS).

Although not a requirement, close proximity to NASA's acoustic equipment eased the logistical difficulties and cost of moving the supporting equipment for the twenty microphones. In addition to the equipment, support staff from NASA's contractor were required to set-up, operate, and disassemble the acoustic equipment each day of measuring. The Wallops facility is within one day's driving time of NASA Langley.

1.5   Site Investigation

To help facilitate planning, and to ensure fulfillment of study requirements while meeting NASA safety requirements, on 7 June, 2000 the study team conducted an initial site investigation of Wallops. During this visit, a location approximately 1000 feet from the west end of runway 10-28 was selected for the acoustic array. Figure 1 below shows the locations of the array, the runway, and the test coordinate system. The video tracking system and meteorological balloon positions are also shown. Safety officers from Wallops were apprised of, and approved, the plan to fly the airplanes through the microphone array at the same altitude above ground level as the highest microphone.

Test Location at Wallops
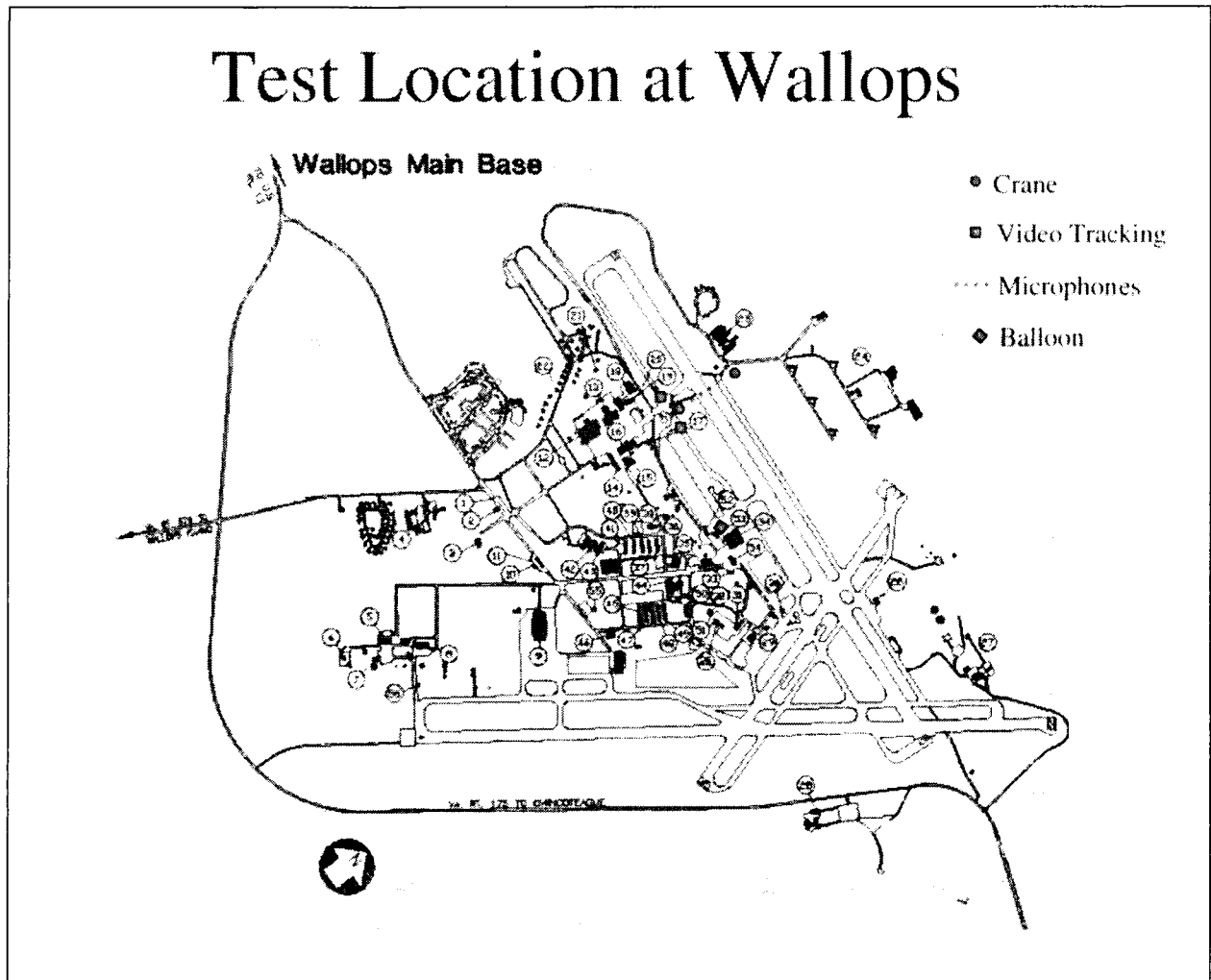
Figure 1. Test Location at Wallops

2   Instrumentation

This section discusses the acoustic instrumentation, the instrumentation used for gathering of time-space-position information (TSPI), the instrumentation used to survey the site and establish a local coordinate system, and other ancillary instrumentation used in the study.

2.1   Microphone Array

The microphone array used in the study was comprised of twenty microphones and their mounting equipment. The mounting equipment included two 230-foot construction cranes and nine poles with microphones 24 feet Above Ground Level (AGL). The origin of the coordinate system for the test was located on the centerline of the runway at the position of the pole-mounted reference microphone and a ground plane microphone. Eight pole mounted microphones, four to the north, and four to the south of the centerline position, extended perpendicular to the runway centerline. The two 230 foot cranes were positioned so that their suspended microphones were a projected distance of 485 feet from the runway centerline, with the highest microphone 200 feet AGL. Each crane supported five microphones. The location of the twenty microphones in the test coordinate system is given in Table 2. A picture of the array is shown in Figure 2. The Figure shows the centerline microphone (number 11) on the right side of the picture, the four northern pole microphones (numbers 12 through 15) in the middle-left of the frame, and the North crane with the five vertical microphones (numbers 16 through 20) on the left side of the picture.

Table 2. Microphone Positions

Microphone Number	Microphone Type	X (feet)	Y (feet)	Z (feet AGL)
1	Vertical Array	0	-425	200
2	Vertical Array	0	-425	162
3	Vertical Array	0	-425	125
4	Vertical Array	0	-425	86
5	Vertical Array	0	-425	45
6	Pole	0	-294	24
7	Pole	0	-203	24
8	Pole	0	-143	24
9	Pole	0	-98	24
10	Ground Board	0	0	0
11	Pole	0	0	24
12	Pole	0	98	24
13	Pole	0	143	24
14	Pole	0	203	24
15	Pole	0	294	24
16	Vertical Array	0	425	45
17	Vertical Array	0	425	86
18	Vertical Array	0	425	125
19	Vertical Array	0	425	162
20	Vertical Array	0	425	200
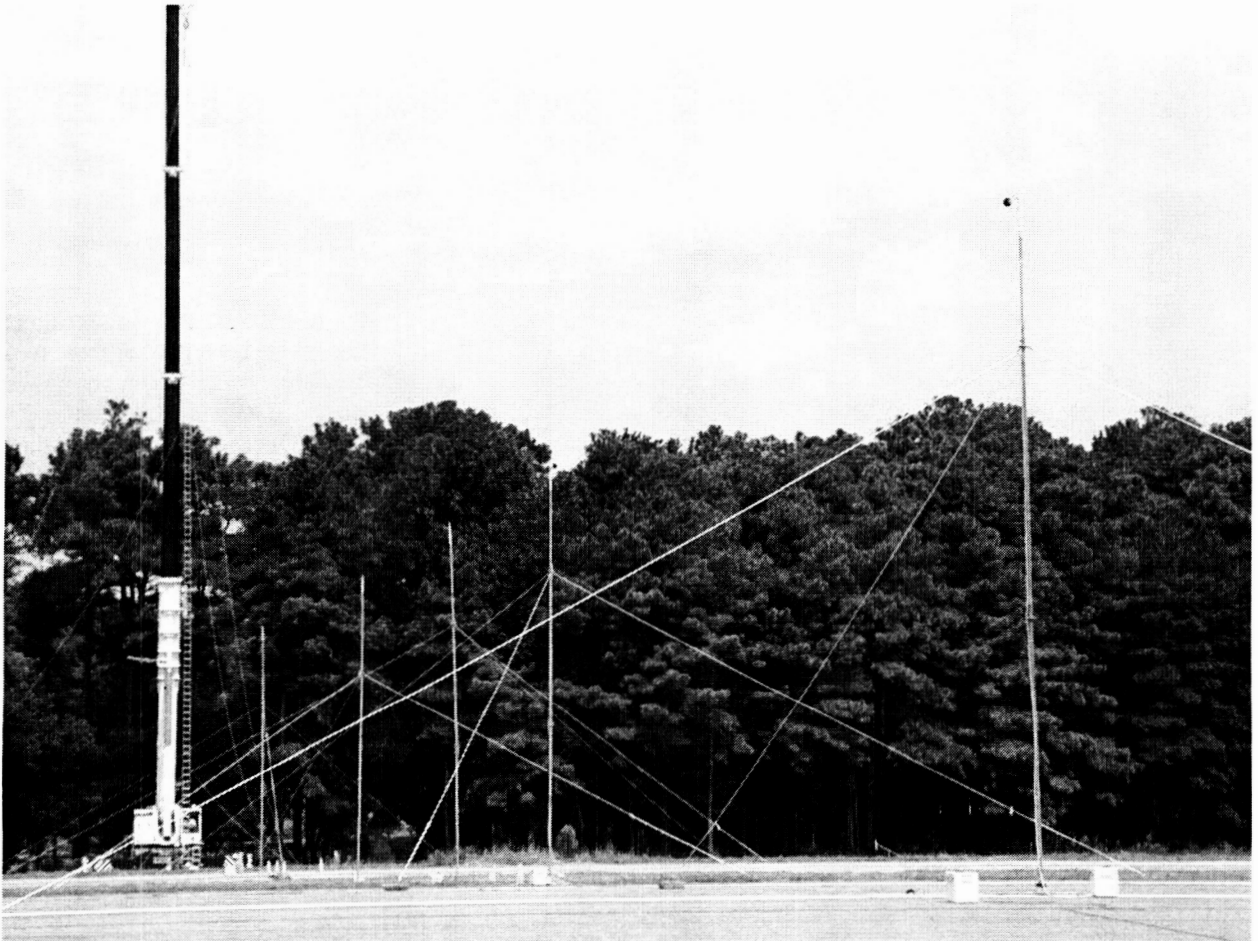
Figure 2. Pole- and Crane-mounted microphones

2.2   Signal Recording System

The acoustic data were collected using two of LaRC's mobile measurement vans. The vans are maintained under contract to LaRC by Wyle Laboratories. One van controlled the ten southern microphones (the five microphones on the southern crane, the four pole-mounted microphones south of the runway centerline, and the ground plane microphone at the runway centerline), the other van controlled the ten northern microphone (the five microphones on the northern cranes, the four pole-mounted microphones north of the runway centerline, and the pole-mounted reference microphone at the runway centerline). Each van was outfitted with a Digital Acquisition Measurement System (DAMS) and collected ten independent channels of acoustic data over a 20 kHz bandwidth. For each channel of the system, the signal was digitized at the microphone, transmitted via cable to the van, multiplexed with time and test run information, and then recorded on an Iomega Jaz drive. The data were transferred from the Jaz drive to an IBM PC for signal processing. The digital acoustic time domain data were transformed to the frequency domain using the average of 5 4096-point fast Fourier transforms (FFTs) with a Hamming window and 50 percent overlap applied, resulting in 1/2-second blocks of data. These FFTs were used to compute narrowband spectra, which were converted to one-third octave-band frequency data. The processed data were stored on compact disk for later off-line reduction and analysis (Section 4). Appendix B discusses the acoustic signal acquisition in more detail.

2.3   Microphone, Preamplifier, and Windscreen

Bruel and Kjaer (B&K) Model 4134 microphones were used in the current study. These are condenser microphones that require a polarization voltage. The polarization voltage was supplied by either a B&K Model 2669 or 2619 preamplifier and a modified version of the B&K Model 2804 power supply. Digitization of the acoustic signal was

performed using a Burr-Brown Model ADC 76KG A-to-D converter. A B&K Model 0237 3.5 inch (9 cm) diameter foam windscreen was placed over each microphone to reduce the effects of wind-generated noise on the microphone diaphragm.

2.4 Acoustic Observer Log

Manual acoustic observer logs were maintained by personnel in the acoustic vans and at the video tracking sites to provide a time synchronized history of observed airplane activity. Ambient noise conditions were also noted on the log sheets.

2.5 Meteorological Instrumentation

At hourly intervals during the flight tests, a tethered weather balloon was released to an altitude of approximately 480 feet above the field. The balloon's instrumentation recorded temperature, pressure, relative humidity, and wind speed and direction. In addition, fixed weather stations on 24 feet AGL poles near the southern and northern cranes also recorded the same data continually during the flight tests. An equipment failure in the tethered balloon led to no altitude-weather data being taken during the DC9 flights. In addition, NOAA meteorological data were collected as a back-up source to the weather balloon data.

2.6 Survey Instrumentation

A site survey was conducted using a differential Global Positioning System (dGPS) which was designed around two single-frequency (commonly referred to as L1) NovAtel® Model RT20E GPS receivers and two GLB® Model SNTR 150 transceivers which facilitate remote communication between the two GPS receivers. The two 25 Watt GLB transceivers were tuned to a frequency of 136.325 KHz.

The dGPS system also contained a Graphical User Interface (GUI) and supporting software that was tailored for use during aircraft noise certification tests. The system is documented in Reference 12.

The dGPS system was used to determine a coordinate system for the measurement instrumentation and the airplane position. This coordinate system was also used in the data processing and analysis. The coordinate system used was defined with the positive X axis running under the departure centerline from Runway 10, the positive Y axis to the north, and the positive Z axis vertically up. All measurement sites, both microphones and video, used this coordinate system. The pole and crane mounted microphone vertical locations were determined by measurement on the particular support system while it was lying on the ground prior to deployment.

2.7 Time-Space-Position Instrumentation

The time-space-position information (TSPI) for the airplanes during the test came from either the dGPS system (discussed in Section 2.6) or a video tracking system. The dGPS TSPI data consisted of time-stamped one-half second position data referenced to the local coordinate system.

The video tracking system includes two digital video camera subsystems and their supporting accessories. Each subsystem recorded airplane events onto videotape that was post-processed to determine the airplane's time and position information throughout the event. Each subsystem consisted of a Canon Optura® digital video camera with a wide-angle lens and the supporting hardware to enable field calibration of the system. The supporting hardware included portable video targets, a camera support structure that permitted the camera to be rotated about all three axes, an optical laser and laser mounting structure, and equipment to accurately determine the geometry of the calibration coordinate system. The accuracy of the video tracking system is within 10 feet of the actual position of the object being tracked at the distances in this test. The video tracking system is discussed in detail in Appendix B.

2.8   Other Instrumentation

Time synchronization of the video tracking equipment was performed using a True Time Model 705 time code generator with a built-in GPS receiver. Universal Coordinated Time (UTC) with a local hour offset was used as the time base for the study.

During measurements, a Radio Shack Model PRO-63 Event Scanner was continuously tuned to the frequency of the Wallops control tower.

Motorola Radius GP300 FM radios were used for communications between the test director and personnel in the acoustic vans and at the video tracking sites. Standard aircraft-band radios were used for communications between the test airplane, the test director, and the Wallops control tower.

3   Field Measurement Procedures

Flight tests with the Beechcraft King Air were conducted on 16 September 2000, the Dassault Falcon 2000 on 27 September 2000, and the DC9 and 767-400 both on 28 September 2000.

3.1   Measurement System Setup

Prior to starting any flight tests, the test site coordinate system was established using the dGPS system discussed in Section 2.6

For safety reasons, the crane and pole mounted microphones were removed from the runway each evening. Therefore, every morning before testing the entire array was completely reassembled. The processes for the daily setting up of the microphones are described below. The processes were identical for the northern and southern portions of the array.

- The crane-mounted microphones were anchored to a steel cable-and-aluminum ladder that had one end attached to the top of the crane. After calibrating the upper microphone, the crane was partially erected so that the next microphone in the array would be about to lift off the ground. This microphone was then calibrated and the process repeated until all five microphones on the particular crane were calibrated. The ladder was guyed to prevent rotation. Figure 3 shows this process. The north crane is in the background in the left of the frame; personnel from Wyle are calibrating the microphones and attaching them to the aluminum ladder in the foreground. The guys used to prevent the ladder from rotating are also visible in the figure. The microphones were oriented for grazing incidence at the average of the nominal elevation angles used in the flight test.
- The pole-mounted microphones were calibrated with the poles lying on the ground. After calibration, the poles were erected and guyed for stability. The microphones were oriented for grazing incidence at the average of the nominal elevation angles used in the flight test.

Figure 3. Ladder Set-up

The video tracking system was also set up and removed each day of measurements. The process for the daily set-up is described below. Appendix C describes this process in greater detail.

- Calibration targets, two for each camera sub-system, were mounted on tripods. The heights of the center of the targets above the reference survey stake were noted for use in post-processing.
- The camera sub-systems were set up. This required mounting the cameras on their tripods and noting their heights above the reference survey stakes, orienting the cameras toward the center of the array, loading new film cassettes, and checking for proper operation.
- The southeastern video site was the control site; the personnel at this site controlled both cameras. The cameras were controlled through their LANC ports and a custom-built control circuit. "Control" in this context means the ability to start and stop recording and to imprint a time-calibration signal onto the film. At this site, a time code generator was connected to the control circuit, and the control circuit was checked for proper operation.

3.2   Flight Procedures

SAE-AIR-1751 uses the same lateral attenuation algorithms for aircraft arrivals and departures. However, if the aerodynamic flow-field around the airplane influences engine installation effects, then the different flap and slat settings used during arrivals and departures suggest that engine installation effects may be a function of airplane configuration. Similarly, it is possible that engine installation effects vary as a function of power setting. For these reasons, a full matrix of power settings and flap/slats configurations was used in the flight test. These configurations included a full power take-off configuration, a de-rate power configuration, a minimum power (approach) configuration, and an aerodynamically clean configuration.

The study objectives require the correlation of airplane configuration parameters (e.g., power, flaps, speed, flight path angle, etc.) and elevation angle (relative to each of the microphones) to the acoustic data. For operations other than level flight (i.e., when the flight path angle is non-zero), comparison of runs becomes difficult since each airplane configuration produces a unique climb angle and hence also unique elevation angles at each point in the operation. This difficulty is eliminated if all flight operations occur at constant altitude (i.e., the flight path angle is zero).

There are two difficulties with using constant altitude for all operations. The first difficulty is that at high thrust settings the airplane will accelerate, but the airspeed range for each fixed configuration with flaps deployed is narrow. Airplanes have minimum speeds dictated by stall speeds plus a safety margin, and maximum speeds dictated by allowable aerodynamic loads on the deployed flaps. For the primary test airplane, the 767-400, with take-off flaps deployed, this airspeed range is on the order of 30 knots. For typical operating weights, the distance required to accelerate these 30 knots was on the same order as the estimated distance the airplane required to fly to obtain sufficient acoustic data (i.e., at least the 10 dB down points). In the flight test, as the airplane accelerated up to the flap retraction speed, the airplane's speed was then held in check, either by climbing or reducing thrust, either of which changed the acoustic signature of the airplane, but this always occurred after the airplane had reached the 10 dB down point.

The second difficulty with constant altitude operations is that changing airspeed causes thrust levels to change. An examination of available data for CF6-80 engines (on an Airbus A-300-600) shows a speed dependence of approximately -56.7 pounds/knot (for comparison, the INM F coefficient for the 767-300 is -53.0 pounds/knot). Over the 30 knot speed increase allowed with take-off flaps, thrust will drop approximately 1700 pounds per engine. If, instead of accelerating, the airplane is allowed to climb at a constant airspeed, the change in thrust will be approximately the same as the change in pressure (about 3.5 percent from sea level to 1000 feet, giving a thrust change of, again, about 1700 pounds). This inherent change in thrust is an issue regardless of whether the test airplane is in level flight or climbing.

During the design of the test, a proposal was made to conduct the low power portion of the test by flying the airplanes at relatively high speed over the microphone array with flaps and landing gear stowed and the engines at approach power. The thrust would be set lower than that required to maintain speed and altitude, so the airplanes would decelerate through the distance required to obtain approximately 10 dB rise and fall for each microphone. This method would have introduced problems of interpretation since this flight procedure would probably result in

different airframe noise than that generated by a normal approach[i]. Rather than obscuring the engine/installation question with issues of airframe noise generation, the requirement of flying the airplane at the exact approach power setting was relaxed, and, instead, the pilots used the lowest thrust setting which allowed the airplane to be stabilized at the same airspeed as the acceleration runs throughout the 10 dB down points.

Table 3 below lists, for each altitude/offset combination, the airplane configurations used during the flight test.

Table 3. Airplane Configuration Series

Configuration Series	Description
100	Full power with take-off flaps, accelerating
200	De-rate power with take-off flaps, accelerating
300	Low power with flaps, constant speed
400	Low power with flaps retracted, constant speed

In order for the speeds of Configuration Series 200 and 300 to be the same at the point where the airplane passed through the array, the take-off flap setting needed to be greater than the low power flap setting. This, combined with the highest weight (early in the test cycle, when the airplanes had maximum fuel), forced the longest acceleration times/distances for Configuration Series 100. Configuration Series 100 also required the pilots to lower the aerodynamic angle of attack as the airplane accelerated in order to maintain altitude. To eliminate variability, the airplanes begin accelerating at the same point throughout each Configuration Series. This was also a requirement of properly flying through the 10 dB down points.

Each of the four airplane Configuration Series shown above was flown at various combinations of altitude and runway offset (Table 4), for a total of 24 passes for each airplane. These combinations were aimed at achieving a maximum number of unique elevation angles with a minimal number of flyovers. Note that some conditions were repeated. In the event a pass contained an error[ii], the pilots flew the pass again, with the pass identifier (the addition of the Configuration and Location series number) incremented by one. Table 4 below lists the offsets and altitudes for the airplane location series.

Table 4. Airplane Location Series

Location Series	Runway offset	Altitude (feet AGL)
10	None (on runway centerline)	400
20	None	400
30	None	280
40	None	200
50	None	200
60	100 feet north of runway centerline	400

Figure 4 below shows the general position of the airplanes and microphones during the passes through the array. The drawing is approximately to scale; the pass at 280 feet AGL is not shown for clarity.

---

[i] The higher speed of this proposed approach would probably have had airframe noise characteristics similar to the general trend for jet aircraft in clean configuration of a 1 dB increase in noise per 10 knot increase in speed. Conversely, jet aircraft airframe noise has been shown to be on the order of 10 dB greater for "dirty" configuration aircraft compared to "clean" (Ref. 13). While the faster, cleaner configuration of this proposed test might have had approximately the same noise levels as the slower, dirtier configuration used in practice, the source of the noise may be significantly different. The airframe noise in the clean configuration is primarily due to turbulent flow over the trailing edge of the wing, while the airframe noise of the dirty configuration is primarily due to vortex shedding from the landing gear and high lift devices.
[ii] Typical errors involved unstable aircraft configurations through the array, high ambient noise during the pass due to vehicle traffic on the runway perimeter road, or miscommunication between the test director and the equipment operators.
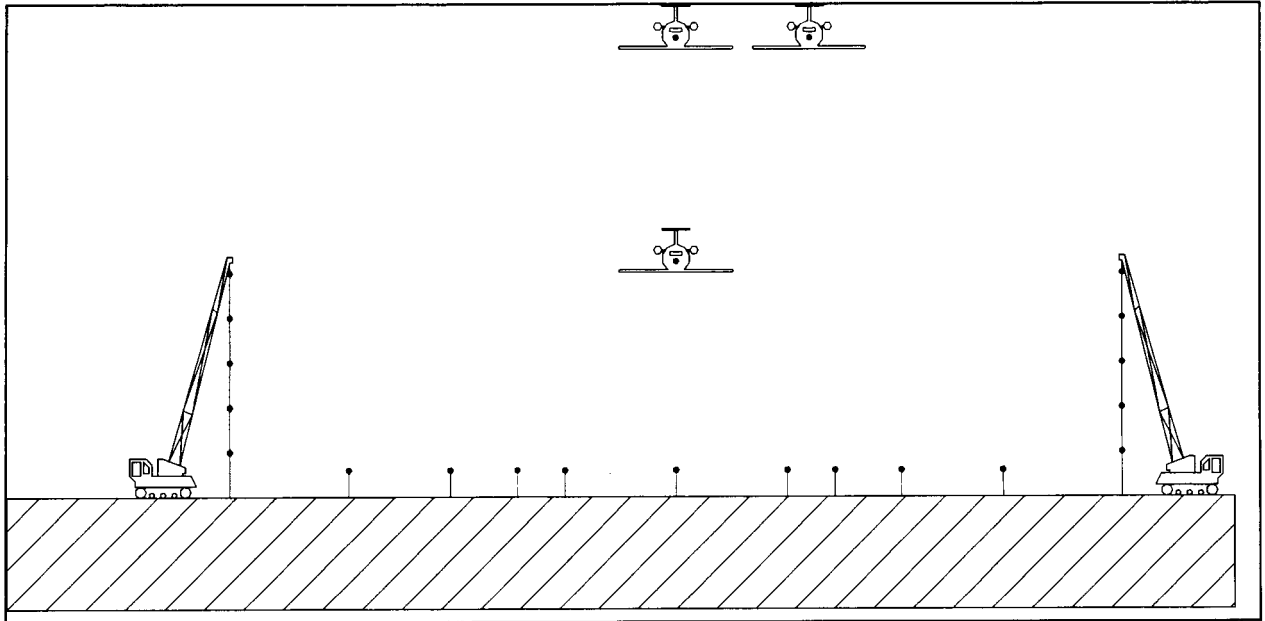
Figure 4. Microphone and Airplane Position Schematic

The following sub-sections describe the airplane configurations used in each Configuration Series. These settings were determined based on discussions with the pilots and review of the operating characteristics of each airplane.

3.2.1   King Air Configuration
Configuration Series 100: 2000 RPM and 2000 ft-lb, take-off flaps, accelerate from 120 to 180 knots
Configuration Series 200: 1710 RPM and 560 ft-lb, approach flaps, accelerate from 113 to 130 knots
Configuration Series 300: 1710 RPM and 1600 ft-lb, flaps up, 200 knots
Configuration Series 400: 1710 RPM and 2180 ft-lb, flaps up, 225 knots

3.2.2   Falcon 2000 Configuration
Configuration Series 100: 81.8% N1, flaps 10, accelerate from V2 + 10 to retract speed
Configuration Series 200: 60% N1, flaps 10, 190 knots
Configuration Series 300: 48% N1, flaps up, 190 knots
Configuration Series 400: 38% N1, flaps up, 190 knots

3.2.3   DC9 Configuration
Configuration Series 100: 2.01 EPR, flaps 5, accelerate from V2 + 10 to retract speed
Configuration Series 200: 1.91 EPR, flaps 5, accelerate from V2 + 10 to retract speed
Configuration Series 300: 1.31 EPR, flaps 5, 225 knots
Configuration Series 400: 1.17 EPR, flaps up, 225 knots

3.2.4   767 Configuration
Configuration Series 100: 102% N1, flaps 15, accelerate from V2 + 10 to 215 knots
Configuration Series 200: 85% de-rate, flaps 15, accelerate from V2 + 10 to 215 knots
Configuration Series 300: 68% N1, flaps 15, 215 knots
Configuration Series 400: 65% N1, flaps 1, 215 knots

3.3   Measurement Procedure
The airplanes flew a continual standard left-hand circuit during the flight test. The pilots set up for each pass during an extended final approach; during this set-up period the test director would coordinate the type of pass and airplane configuration with the pilots. When the airplane approached the array, the pilots alerted the test director, who then called for the acoustic and video tracking personnel to initiate data collection. The pilots held the airplane configuration from approximately 40 seconds prior to reaching the array to approximately 20 seconds after passing

through the array. After the airplane passed through the array, the test director called for the acoustic and video personnel to stop recording. The airplane turned left base, then left downwind. While downwind, the test director checked with all test personnel to determine if any problems occurred during the pass. If a problem occurred, the pass was re-run. If the pass had no known problems, the test director called for the pilots to prepare for the next pass. The pilots turned left base to final and the process was repeated.

Each configuration series was flown in the order of the location series given in Table 4. This order was used for safety reasons; the pilots could first familiarize themselves with the configuration during the highest altitude (400 feet AGL) runs on the runway centerline and then descend to lower altitudes on subsequent passes. The last pass of each configuration series was conducted with the aircraft at 400 feet AGL and offset from the runway centerline. These offset passes were considered the most difficult because they provided the pilots with the fewest visual cues for tracking.

4   Data Reduction and Analysis

4.1   Data Reduction Process

A suite of computer programs was used to facilitate data reduction. The organization of this suite of programs and the data flow from one program to the next is presented below in Figure 5.
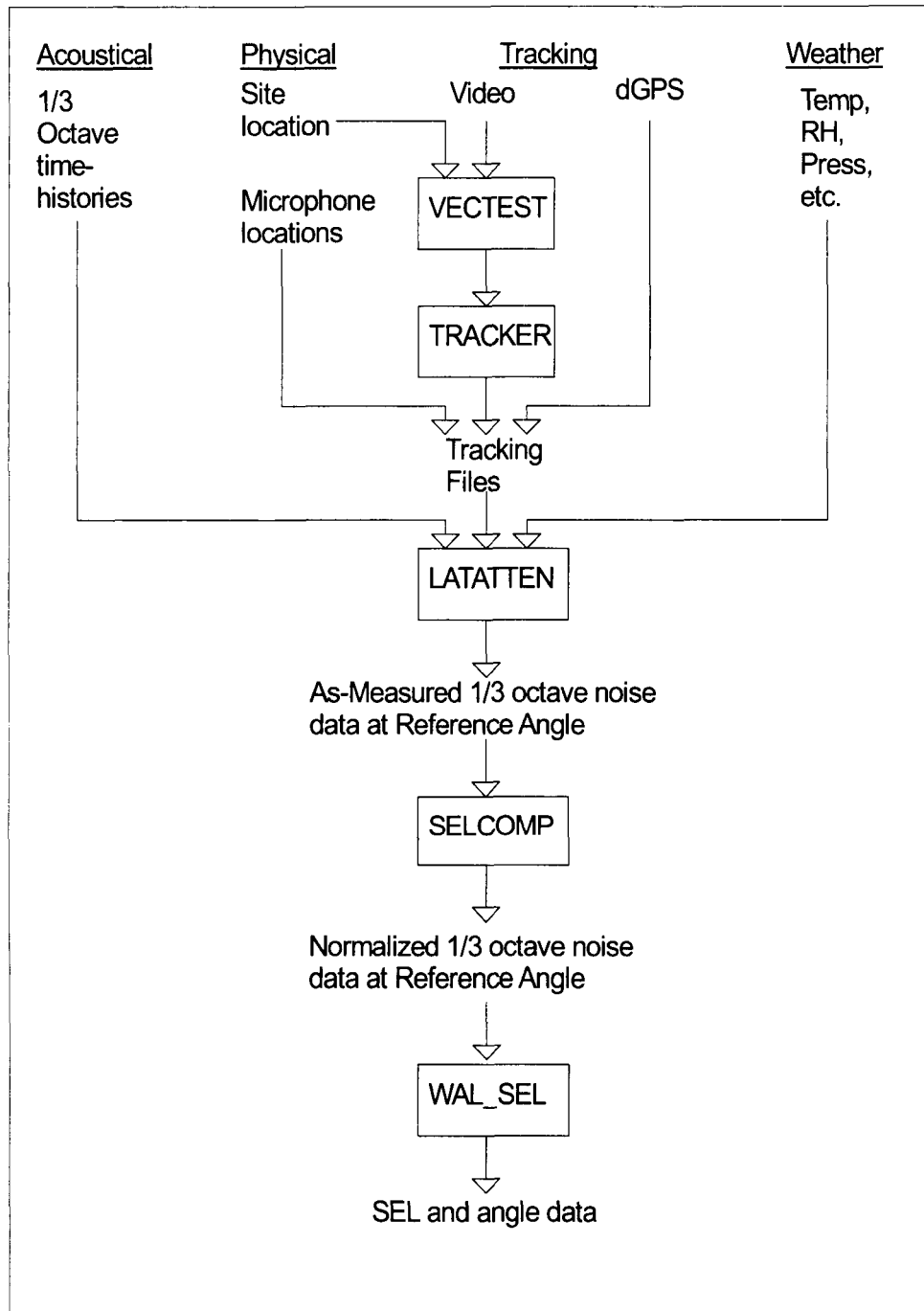

Figure 5. Flow Diagram of Data Reduction Process

Three data sets are used as inputs: acoustical data, tracking data, and meteorological data. The acoustical data are comprised of time-stamped, half-second one-third octave-band data; the tracking data are comprised of either video or dGPS tracking data; and the meteorological data are comprised of time-stamped temperature, relative humidity, atmospheric pressure, wind speed and direction. The following sections describe each program used in the data reduction process.

4.2   Tracking Data Reduction

Data reduction for the video system involves converting the digital image of the airplane recorded by the two cameras to emission time and three-dimensional position information used by other data reduction programs. This conversion is described in Reference 14. The output of the process is an ASCII format text file for each pass. The tracking data from the dGPS system are in the dGPS systems ASCII text format. The data were taken from this format and converted to the format of the tracking system (also ASCII text files).

The video tracking data provides approximately four seconds of tracking data centered on the airplane passing through the array. These four seconds are not adequate to provide all the tracking data needed for the SEL metric; therefore, an extrapolation program was written to extend the flight track data. This extrapolation program calculates where the airplane passed through the array (when x=0) and the speed of the airplane at this point. The program then calculates prior and future positions based on this intercept position and speed. This program was not needed with the dGPS system since the airplane was continually tracked.

4.3   Data Reduction and Coordination Programs

These programs extract the one-third octave-band noise data from the acoustic files, coordinate the time of reception with the weather files and the tracking files, calculate the emission times and angles, and provide an SEL normalized to a fixed distance and fixed range of emission angles by correcting for spherical spreading, atmospheric absorption, and ground effects. The steps in the process are described below.

4.3.1   Time-based to angle-based conversion

In order to account for the differences in distance between the various microphones and the aircraft flight track, the acoustic data for the non-reference microphones were selected to contain the same range of emission angles from the airplane as the reference microphone. Thus, the acoustic time history for each microphone encompassed the same range of fore-aft emission angles. For measurement points with the same emission angle from the source, but at different distances, standard acoustic propagation techniques can be used to correct to a common distance. Correcting to common emission angles becomes a way of eliminating differences in the durations of the acoustic time histories. These duration effects were minimal given the similar distances from the airplane to each microphone in the array. The steps in the LATATTEN program which correct for duration effects are:

- Find the emission angle and propagation time from the airplane to each microphone for each time step in the pass.
- At each reception time step and for each microphone, find the corresponding emission time, and the aircraft position and emission angle.
- For the reference microphone find the emission angle at each time step. For each non-reference microphone find the time step with the same (or closest) emission angle. Thus, for each time step of the reference microphone signal, generate a sequence of spectra for each non-reference microphone signal corresponding to the emission angles of the reference microphone
- Write out the sequence of the aircraft positions and received spectra emitted at the same angle as the reference microphone.

Figure 6 below shows a schematic of an airplane approaching the microphone array. The two airplane images represent the same craft but at different times during a single pass. Only a single sideline (non-reference) microphone is shown for clarity, instead of the entire U-shaped array. The airplane-to-microphone emission angle at any position is $\tan^{-1}\left(\sqrt{z^2 + y^2}\Big/x\right)$. For the example shown, the airplane at position "A" has the same emission angle to the reference microphone as the airplane at position B has to the non-reference microphone. After

correcting for propagation differences, the data collected for the reference microphone at position "A" can be compared to the data collected for the non-reference microphone at position "B".
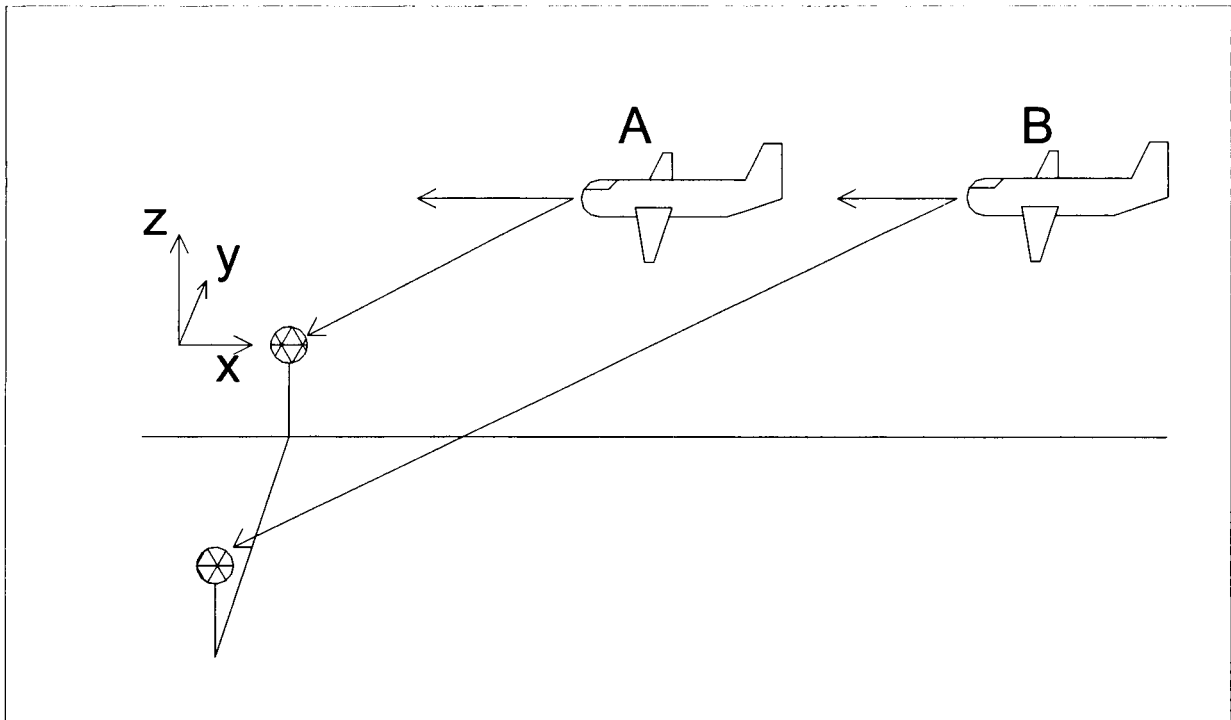

Figure 6. Duration Correction schematic

4.3.2 Propagation and Ground Effects Program

This program calculates the known propagation effects from the airplane to each of the microphone locations, normalizes these data to the reference microphone distance and returns the sound level difference between the normalized data and the reference microphone. The known propagation effects are the spherical spreading of sound from a point source $[20\log_{10}(d/d_{ref})]$, and atmospheric absorption of sound as a function of frequency. The atmospheric absorption of sound was computed using International Standard Organization's ISO 9613-1; data corrected using ISO 9613-1 are presented in subsequent sections. The program also calculates the ground effect using the algorithms of Embleton, Piercy, and Daigle (Ref. 15). Those microphones located on or over the runway used a flow resistivity of 20,000 c.g.s Rayls; the microphones mounted over grass used a flow resistivity of 150 c.g.s. Rayls.

The reference microphone used in this study was generally the pole-mounted microphone at the runway centerline. For those operations flown offset to the north of the runway centerline, the microphone with the highest elevation angle (i.e., the microphone most directly below the airplane) was used as the reference microphone; Table 5 through Table 8 below show the pass identification, time the airplane was at the closest point of approach (CPA) to the reference microphone, the airplane position as it passed through the array (at $X \sim 0$), the identification number of the selected reference microphone, and the elevation angle at CPA relative to the reference microphone. Engine installation effects are quantified by comparing the data from the nineteen other microphones to the data from the reference microphone.

Note that in Table 7, the DC9 pass information, passes 110 through 240 have Y values of zero and elevation angles of 90 degrees at the CPA. One of the video tracking cameras failed during these events; because of this failure, an exact airplane position could not be determined. However, for the passes down the centerline of the runway, a reasonable approximation of the airplane position is assumed to be somewhere in the Y=0 plane. An examination of the later passes shows that this assumption may be in error on the order of twenty feet or so, which is comparable to the random error inherent in the video tracking system. DC9 Event 160, a run offset from the runway centerline, had to be discarded because, given the wide variation in the other sixty-series passes, a reasonable assumption about

the plane of the airplane's travel could not be made.

Table 5. King Air Pass Information Table

ID	Time	Y (feet)	Z (feet)	Ref. Mic	Elevation
111	9:46:44.67	6.0	402.1	11	89.1
120	9:51:25.84	24.3	392.5	11	86.2
131	10:00:14.09	15.9	230.4	11	85.6
140	10:04:35.80	33.1	163.5	11	76.6
150	10:08:31.44	15.6	165.0	11	83.6
160	10:13:44.72	108.1	355.1	12	87.7
211	10:29:39.56	20.6	362.2	11	86.5
220	10:34:32.12	21.7	383.4	11	86.5
230	10:39:42.14	9.4	258.6	11	87.7
240	10:50:11.61	17.7	138.0	11	81.2
250	10:55:26.11	18.9	180.5	11	83.1
260	11:00:10.96	117.9	350.1	12	86.6
310	11:04:50.44	29.9	347.9	11	84.7
320	11:09:05.44	24.4	359.4	11	85.8
330	11:13:19.13	13.5	220.5	11	86.1
341	11:22:58.21	16.2	138.0	11	81.9
351	11:32:38.21	25.1	157.5	11	79.4
360	11:37:34.12	111.5	359.8	12	87.8
410	11:42:34.46	115.9	286.9	11	66.2

Table 6. Falcon 2000 Pass Information Table

ID	Time	Y (feet)	Z (feet)	Ref. Mic	Elevation
112	9:55: 9.79	-1.7	431.5	11	89.8
120	10:00:42.07	23.5	433.3	11	86.7
130	10:06:34.67	-20.8	316.6	11	85.9
141	10:18:32.34	-6.6	211.6	11	88.0
150	10:23:52.41	-20.5	217.9	11	84.0
210	10:38:25.49	27.6	411.0	11	85.9
220	11:26:34.43	9.3	397.5	11	88.6
230	11:30:06.79	1.9	280.1	11	89.6
240	10:42:47.97	-23.3	185.9	11	81.8
250	10:46:50.26	-1.2	190.5	11	89.6
260	11:33:42.33	73.9	383.5	12	86.2
310	10:50:41.40	-8.5	401.9	11	88.7
320	11:37:32.13	4.3	409.4	11	89.4
330	11:41:41.43	-14.0	285.6	11	86.9
341	10:58:53.18	2.7	214.2	11	89.2
351	11:06:39.01	-26.6	204.9	11	81.6
362	12:04:18.92	68.1	363.9	12	85.0
410	11:10:40.22	32.6	416.6	11	85.3
420	11:50:19.78	-0.6	407.8	11	89.9
430	11:53:46.38	-14.2	277.3	11	86.8
440	11:14:16.40	-0.1	211.5	11	90.0
451	11:21:36.64	-24.7	199.4	11	82.0
460	11:57:07.31	120.1	413.4	12	86.8

Table 7. DC9 Pass Information Table

ID	Time	Y (feet)	Z (feet)	Ref. Mic	Elevation
110	16:17:43.02	0.0	353.8	11	90.0
121	16:25:52.62	0.0	369.6	11	90.0
130	16:29:55.31	0.0	292.1	11	90.0
140	16:34:25.13	0.0	194.1	11	90.0
150	16:38:48.75	0.0	188.5	11	90.0
210	16:47:38.45	0.0	415.9	11	90.0
220	16:52:05.15	0.0	405.4	11	90.0
230	16:56:29.92	0.0	295.8	11	90.0
240	17:00:55.14	0.0	202.3	11	90.0
250	17:05:16.21	-24.8	192.8	11	81.6
260	17:09:35.19	100.7	441.1	12	89.6
310	17:13:38.71	11.2	425.8	11	88.4
320	17:17:49.20	-28.7	411.2	11	85.8
330	17:21:37.11	11.9	303.4	11	87.6
340	17:25:39.75	-15.5	197.9	11	84.9
351	17:33:54.11	-11.4	197.5	11	86.2
360	17:38:11.95	62.6	406.2	12	84.7
410	17:42:28.21	-8.9	394.5	11	88.6
420	17:46:56.46	25.6	411.9	11	86.2
440	17:51:19.87	3.7	192.5	11	88.7
450	17:55:42.48	16.9	181.9	11	83.9
460	18:00:08.69	25.5	384.2	11	86.0

Table 8. 767 Pass Information Table

ID	Time	Y (feet)	Z (feet)	Ref. Mic	Elevation
112	12:51:14.12	4.7	427.3	11	88.9
121	13:04:24.44	0.6	413.9	11	89.0
130	13:10:34.43	9.6	317.7	11	88.0
140	13:16:44.34	-4.9	203.5	11	88.4
150	13:22:14.11	-9.2	198.1	11	86.9
160	13:27:51.92	69.0	442.5	12	86.0
210	13:34:43.45	1.3	416.3	11	89.5
221	13:45:01.23	1.7	416.6	11	89.8
230	13:50:06.48	11.8	234.3	11	86.7
240	13:55:23.03	23.3	219.5	11	83.2
250	14:00:22.77	16.4	222.1	11	85.3
260	14:05:08.38	144.6	432.3	13	89.2
310	14:12:55.77	3.4	416.2	11	89.5
321	14:22:06.44	-1.4	390.2	11	89.7
330	14:26:37.51	-8.7	389.3	11	88.5
340	14:31:07.48	19.4	201.3	11	83.8
350	14:35:40.26	1.9	197.6	11	89.3
360	14:40:34.00	115.0	388.4	12	87.3
410	14:45:23.83	22.7	386.6	11	86.4
430	14:54:31.26	-8.4	284.7	11	88.2
440	14:58:36.91	-3.0	193.5	11	89.0
450	15:02:28.87	2.5	187.7	11	89.0
460	15:06:29.65	116.8	406.4	12	87.2

4.4   Summary graphics

This section presents graphics that show the engine installation effect for each airplane in the study. The graphics in these sections represent the entire series of passes. Graphics for the individual series for each airplane are presented in Appendix D. Also shown in each Figure is the long-range, air-to-ground attenuation algorithm of SAE-AIR-1751.[iii]

4.4.1   King Air Engine Installation Effects

Figure 7 below shows all the engine installation effects data collected during the entire flight test for the Beechcraft King Air; this figure also contains the SAE-AIR-1751 air-to-ground curve included for comparison. Engine installation effects for the Beechcraft King Air for each Configuration Series are shown in Figure 20 through Figure 23 of Appendix D.
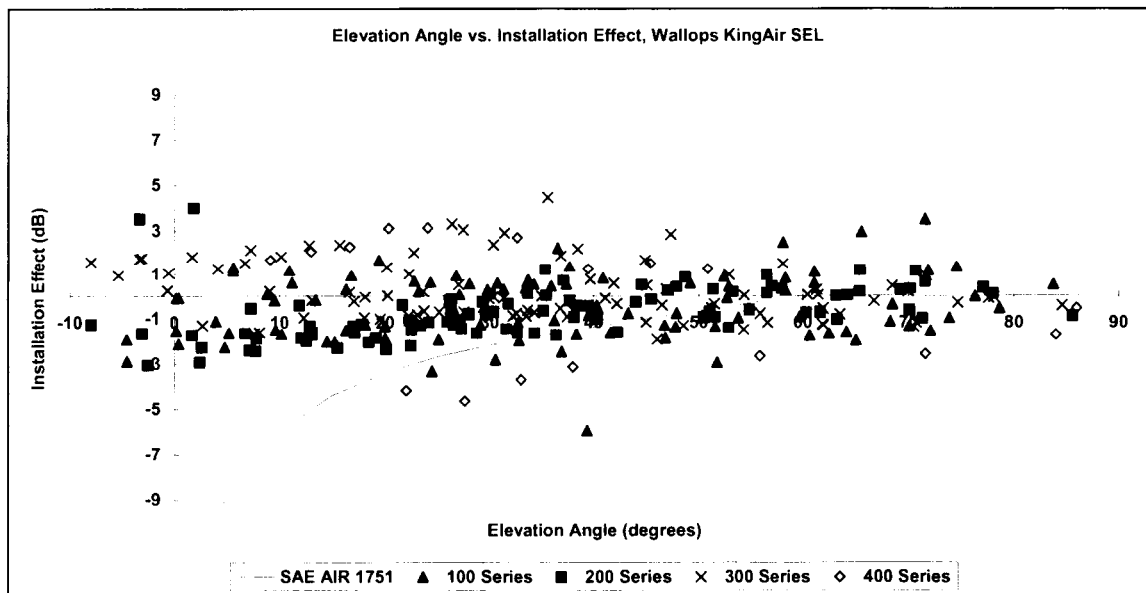

Figure 7. King Air Installation Effect, all passes

4.4.2   Falcon 2000 Engine Installation Effects

Figure 8 below shows all the engine installation effects data collected during the entire flight test for the Falcon 2000; this figure also contains the SAE-AIR-1751 air-to-ground curve included for comparison. Engine installation effects for the Falcon 2000 for each Configuration Series are shown in Figure 24 through Figure 27 of Appendix D.

[iii] The SAE-AIR-1751 algorithm is divided into two equations; one represents the component of lateral attenuation when the source aircraft is on the ground (ground-to-ground propagation), the other represents the component of lateral attenuation when the aircraft is in the air (air-to-ground propagation). For short ranges (less than 914 meters, or about 3000 feet) when the aircraft are in the air, SAE-AIR-1751 combines the two equations. The long ranges (greater than 914 meters) when the aircraft is in the air, SAE-AIR-1751 uses only the in-air component. Although the CPA source-to-receiver distances in the Wallops test were always less than 914 meters, the test was designed with the microphones located sufficiently above the ground plane so that ground effects would occur at frequencies lower than those that significantly contribute to A-weighted sound levels. The short range SAE-AIR-1751 algorithm, which contains the ground-to-ground component of lateral attenuation, is therefore not presented in the following Figures.
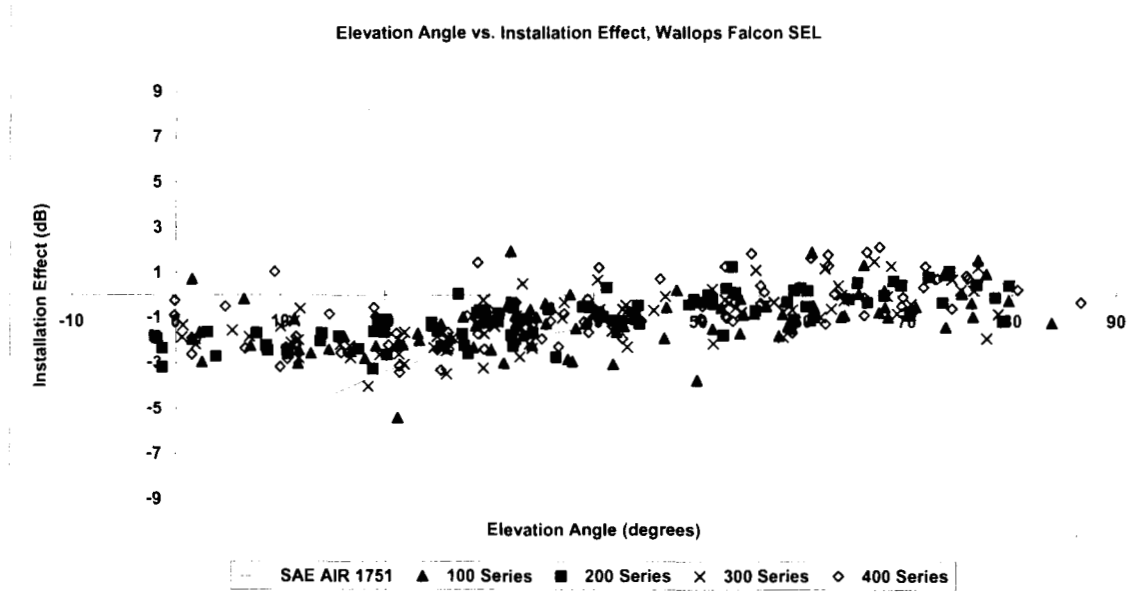
Elevation Angle vs. Installation Effect, Wallops Falcon SEL

Figure 8. Falcon 2000 Installation Effect, all passes

4.4.3   DC9 Engine Installation Effects

Figure 9 below shows all the engine installation effects data collected during the entire flight test for the DC9; this figure also contains the SAE-AIR-1751 air-to-ground curve included for comparison. Engine installation effects for the DC9 for each Configuration Series are shown in Figure 28 through Figure 31 of Appendix D.

Elevation Angle vs. Installation Effect, Wallops DC9 SEL

Figure 9. DC9 Installation Effect, all passes

4.4.4   767-400 Engine Installation Effects

Figure 10 below shows all the engine installation effects data collected during the entire flight test for the 767-400; this figure also contains the SAE-AIR-1751 curve included for comparison. Engine installation effects for the 767-400 for each Configuration Series are shown in Figure 32 through Figure 35 of Appendix D.
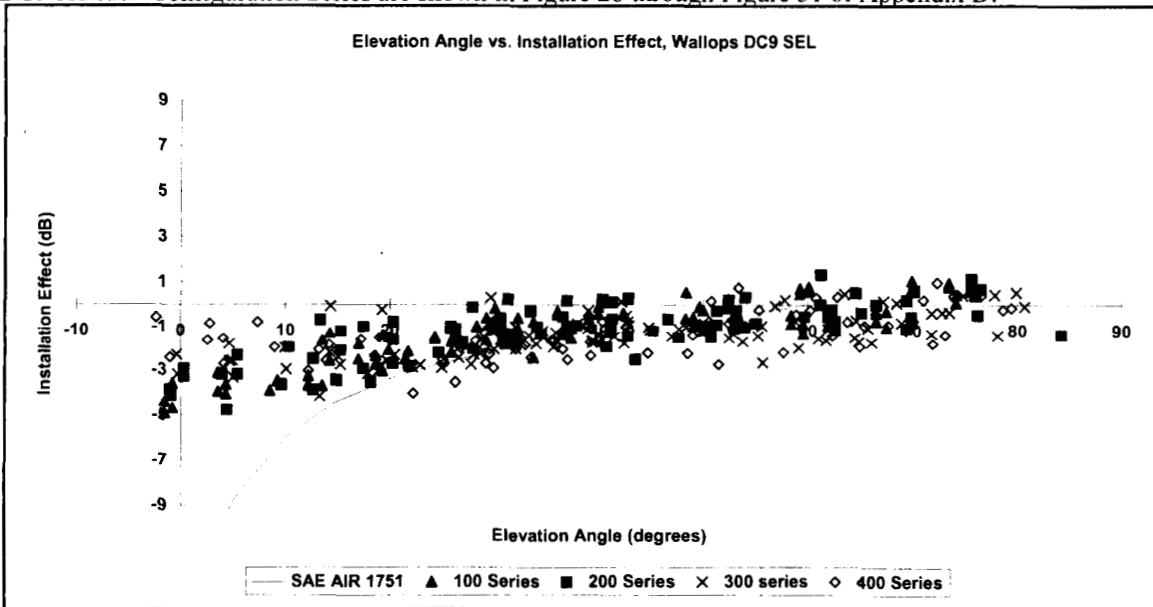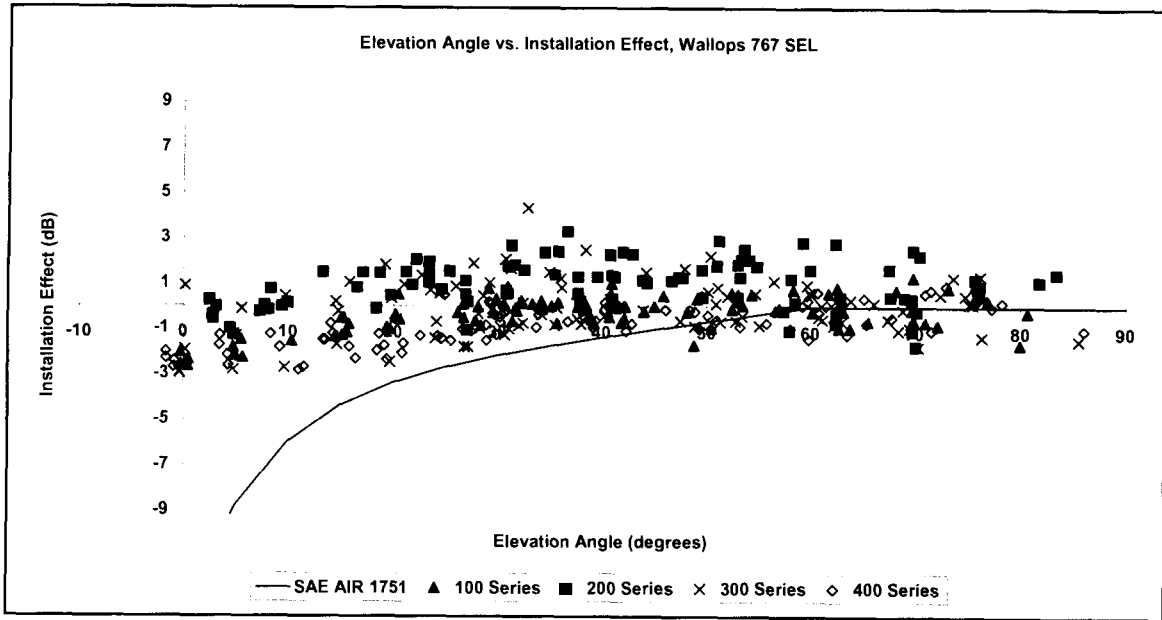
Figure 10. 767-400 Installation Effect, all passes

4.5   Discussion of Results

The data presented in Section 4.4 show significant differences in the engine installation component of lateral attenuation between jet airplanes with wing-mounted engines and jet airplanes with tail-mounted engines. Possible reasons for these differences are related to the differences in physical geometry of these two groups of airplanes. In addition, virtually no engine installation effects are seen for propeller-driven airplanes.

4.5.1   Airplanes with Tail-Mounted Engines

Noise generated by jet engines has a number of discrete sources, including the fan, the compressor and turbine machinery, the combustor, and primary (jet) and secondary (fan) exhausts. These noise sources tend to be directional. The fan noise generally propagates forward, the machinery and combustor noise propagates perpendicularly, and the exhaust noise tends to propagate to the rear.

When airplanes with tail-mounted engines are perpendicular to the receiver at low angles, the fuselage and/or tail section visually shields the farthest engine. With complete acoustic shielding of the farthest engine, theory indicates that the noise should be reduced 3 dB ($10\log(\frac{1}{2}) = -3$) for a two-engine airplane. This -3 dB represents an upper limit to the amount of shielding; jet mixing noise will occur behind the engines, and the farthest engine will be visible to the receiver after the airplane passes the point of closest approach, which will reduce the magnitude of the shielding. While the jet mixing noise occurs behind the engines, the closest jet itself acts as a shield to the farthest jet. (Appendix E presents a simple geometric model of this jet shielding.) Hodge[16] has noted that additional attenuation may be due to scattering of the engine noise as it encounters the wing down-wash and the wingtip vortices. These effects, combined with the shielding of the farthest engine, presumably account for the attenuation at low angles seen in Figure 8 and Figure 9.

For the DC9, a study airplane with tail-mounted engines, engine installation effects are evident below about 60 degrees. The trend for the DC9 is in general agreement with the SAE-AIR-1751 air-to-ground algorithm above about 30 degrees. The good agreement between DC9 and SAE-AIR-1751 is not surprising, given that SAE-AIR-1751 was dominated by data from flight tests with Boeing 727 airplanes, which have three co-planar tail-mounted engines, an arrangement generally similar to that of the two-engined DC9.

The results for the Dassault Falcon 2000 resemble those of the DC9; small values of attenuation below about 50 or 60 degrees, but with somewhat less attenuation at the lowest angles. Based on this observation that the engine installation effect for the DC9 (low bypass ratio) and the Falcon 2000 (high bypass ratio) are similar, engine bypass ratio does not appear to be an important variable.

4.5.2   Airplanes with Wing-Mounted Engines

For modern large civil transport airplanes with wing-mounted engines, the engines are mounted either slightly forward of or directly under the wing. The basic mechanisms of jet shielding are the same as for the airplanes with fuselage-mounted engines; shielding and reflections by the aircraft structure and interactions with flow fields. However, the wing-mounted location provides limited opportunity for noise from the engines to be shielded by airplane surfaces. Note that blocking or shielding of the noise from one or more engines will cause an increase in the magnitude of lateral attenuation, while reflections will cause an apparent amplification.

For the 767, the study airplane with wing-mounted engines, engine installation effects are evident at   elevation angles below about 20 degrees (see Figure 10). This is in contrast to the behavior observed for the DC-9 and the guidance of SAE-AIR-1751.

4.5.3   Airplanes with Propellers

The King Air data, as presented in Figure 7, display no discernible engine installation effects. The substantial scatter in the data is expected due to the tonal nature of propeller noise, resulting in constructive and destructive interference between sound from the two propellers and the reflections from the ground.

4.6   Aircraft Configuration Influence on Engine Installation Effects

One of the study objectives listed in Section 1.2 was to identify the airplane and engine parameters that affect lateral attenuation. This was the reason the four different airplane configurations described in Section 3.2 were flown. To examine whether airplane and engine parameters influence engine installation effect (and, hence, lateral attenuation), a comparison of the differences between the different series was made. The comparison for the DC9 and the 767 are discussed below.

4.6.1   DC9 Airplane Configuration

Figure 11 below shows a 95% confidence interval comparison of the four different pass series individually and in combination for the DC9. The confidence intervals are based on the data within 10-degree bands. I.e. for a given series of flights the average installation effect is plotted at the average elevation angle within each 10-degree band. The limits of the confidence intervals are displayed in the Figures as the error bars surrounding the mean value. Displaying the confidence intervals this way emphasizes the variation with elevation angle. The size of the confidence intervals remains relatively constant across the range of elevation angles, with no obvious trends.

There is little difference between any of the series except at the lowest angles, 0-10 degrees, for which the 100 series and the 400 series lay, respectively, below and above the combined series. This difference does not occur for the 10 to 20 degree range, suggesting that there is probably no systematic effect of aircraft configuration on the measured engine installation effect. Thus, given the relatively tight grouping of the confidence intervals (except at 0 to 10 degrees), it is believed that the combined series adequately represents the engine installation effect of the different airplane configurations of the DC9.
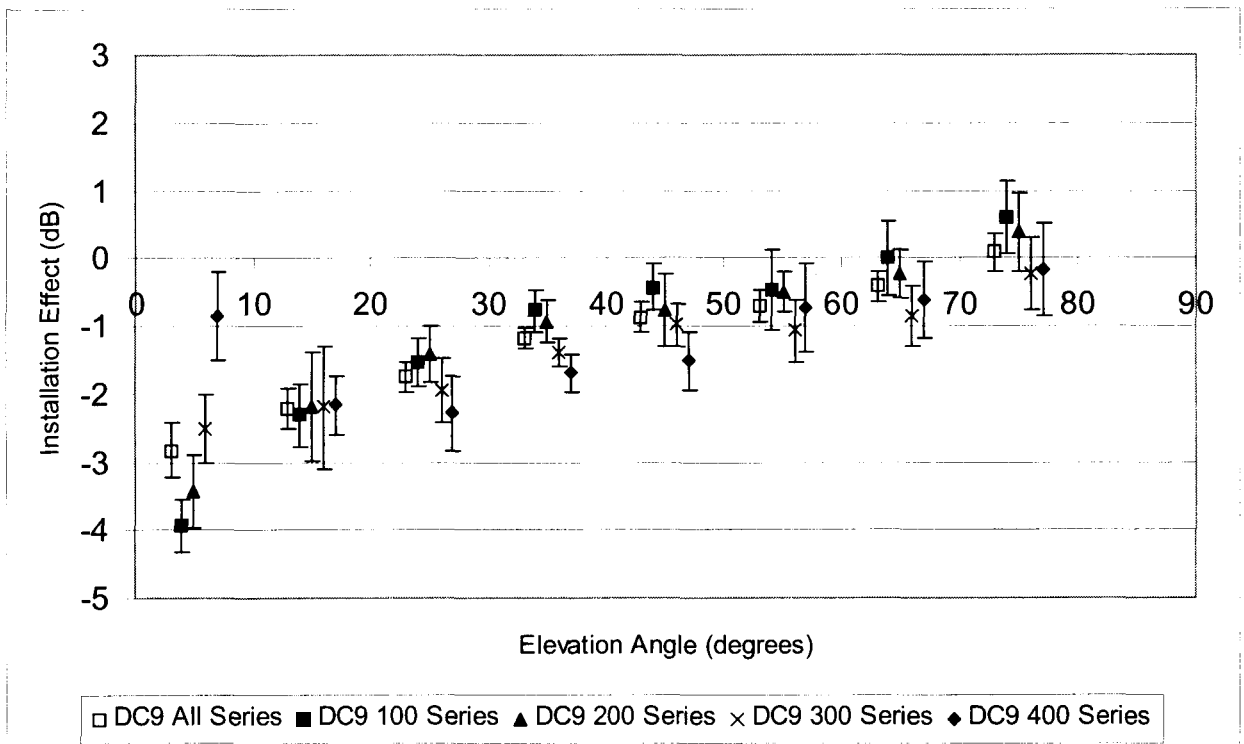

Figure 11. 95% Confidence Intervals for DC9 pass series

4.6.2   767 Airplane Configuration

Figure 12 below shows a confidence interval comparison of the four different pass series and the combined series for the 767. As with the DC9, the confidence intervals are based on the data within 10-degree bands.

Unlike the DC9, the 767 contains a series which consistently lies outside the range of the other confidence intervals;

the 200 series data fall above the combined 100, 300, 400 series confidence interval limits at every elevation angle below 60 degrees. The other three series (100,300,400) fall within the range of the combined confidence intervals, with the exception of the 400 series in the 30 to 40 degree range.

Further examination of the 200 series data showed a significant difference in the spectral content of this series compared those of the others. Figure 13 shows the spectral content at CPA of pass 130, a full power pass over the center of the runway, for microphones 11 (the reference) microphone and microphone 6, a pole mounted microphone. The spectra are "as measured," or uncorrected for spherical spreading, atmospheric attenuation, and ground effects (duration effects aren't an issue for non-integrated metrics). The spectra appear as expected, with the farther microphone, number 6, exhibiting lower sound pressure levels than the closer, reference microphone. Figure 14 shows the uncorrected spectral content at CPA of pass 230, a de-rated power pass over the center of the runway, again for microphones 11 and 6. In this pass, the aircraft produces distinct high frequency content between bands 35 and 39 (3150 and 8000 Hz). This high frequency content significantly influences the results of the analysis. While the de-rated power passes for this airplane do exhibit the engine installation effects shown in Figure 12 (and Figure 33), the high frequency content of these series may be due to a unique characteristic of the Boeing 767-400 flight test airplane (e.g., an open bleed valve at these flight conditions) and therefore should not necessarily be considered typical of other aircraft with wing-mounted engines. For this reason, the 200 series data will not be further considered for these analyses.

If the 200 series is dropped from consideration, then the remaining three series fall within the range of the combined confidence intervals, with the exception of the 400 series in the 30 to 40 degree range. Given the overlap of the confidence intervals (except at 30 to 40 degrees), it is believed that the combined series adequately represents the engine installation effect of the different airplane configurations of the 767.
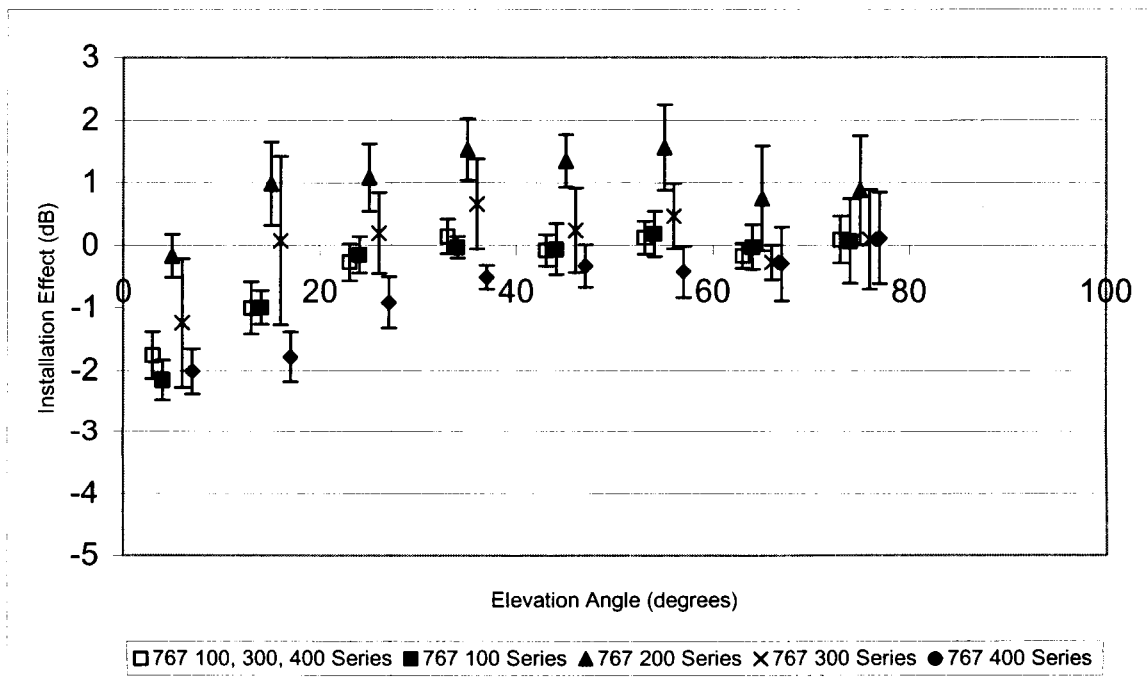

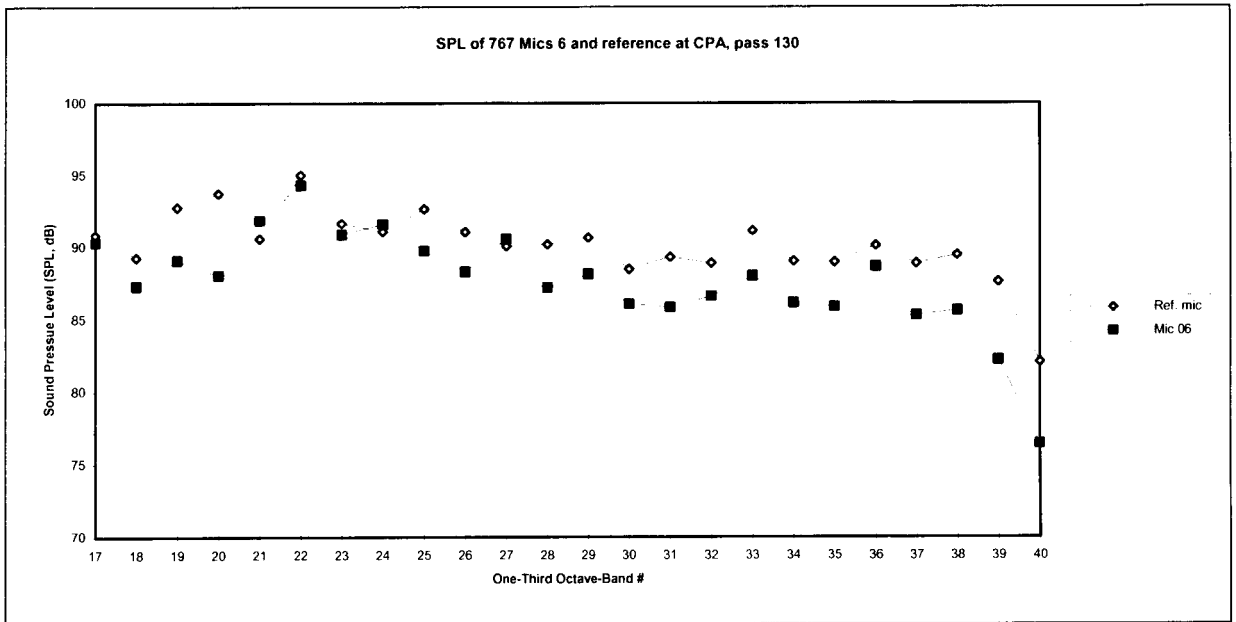Figure 12. 95% Confidence Intervals for B767 pass series

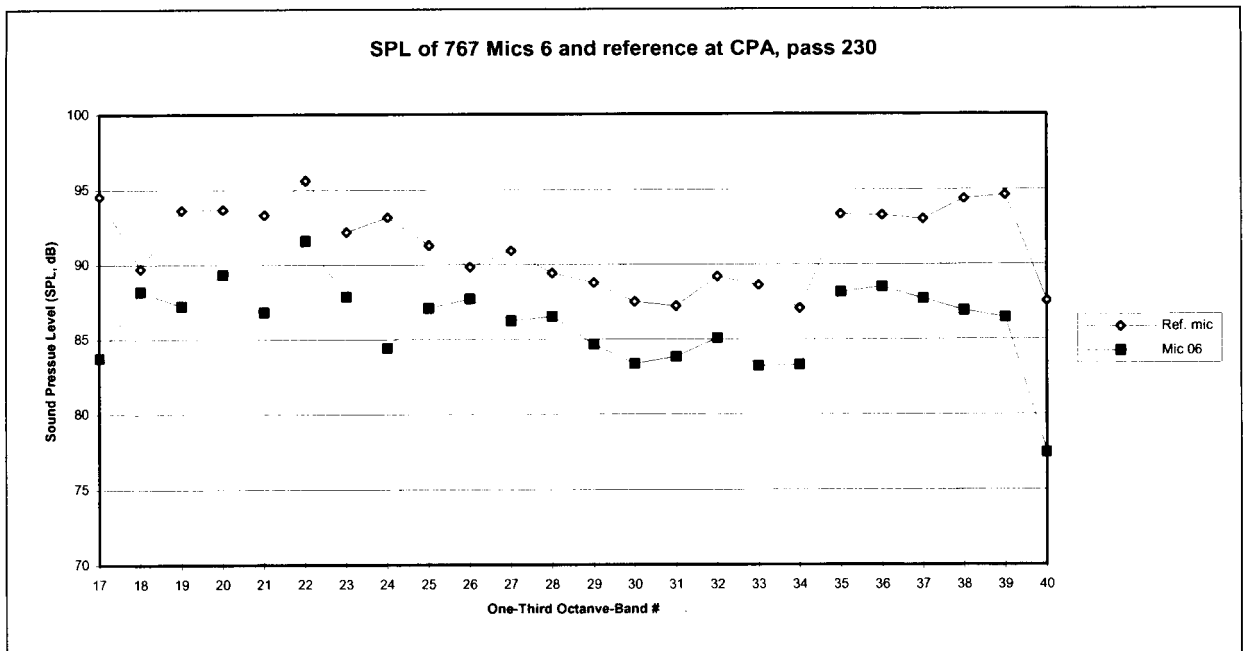Figure 13. Uncorrected spectrum at CPA, 767 pass 130

Figure 14. Uncorrected spectrum at CPA, 767 pass 230

4.7   Proposed Engine Installation and Ground Effects Algorithms

This section presents a method of using an engine installation algorithm, based on the algorithms of SAE-AIR-1751, to generate a new lateral attenuation algorithm that incorporates both ground effects and engine installation effects of either wing- or tail-mounted engines. Appendix E describes a different engine installation algorithm based on an empirical jet shielding model.

4.7.1 Ground Effects in SAE-AIR-1751

The existing long-range SAE-AIR-1751 lateral attenuation equation[iv], $-9.9e^{-0.13\theta} + 0.066\theta - 3.96$, is dominated at low angles by the exponential term $-9.9e^{(-0.13\theta)}$. The two other terms are linear or constant. Because ground effects dominate at low angles, this exponential term can be considered to be the ground effects term. The magnitude of the ground effects at low angles is determined by the value of the leading constant (-9.9). Changing this leading constant provides a way to scale the ground effects component.

The results presented in this section correspond to the long range (distance > 914 m) air-to-ground lateral attenuation equation in SAE-AIR-1751. The transition of long range air-to-ground lateral attenuation and the over ground attenuation is given in SAE-AIR-1751 as $\Lambda(\theta,l) = G(l)\Lambda(\theta)/13.86$. For the new equations where the ground effect (GE) and engine installation effects (IE) are separated, the transition equation becomes $\Lambda(\theta,l) = G(l)(GE(\theta) + IE(\theta))/13.86$.

4.7.2 Tail-mounted Engine Installation Algorithm

The SAE-AIR-1751 equation can be modified based on the experimental data collected in this study. If the same form of the equation is used, $Ae^{-0.13\theta} + C\theta + D$, the coefficients can be found from a least squared error fit to the empirical data. These empirical engine installation parameters produce the small dashed line labeled "Tail-only-EI" shown below in Figure 15; the values of the coefficients are given in Table 9 below. The resulting engine installation algorithm can be combined with a scaled version of the ground effect equation to produce a new lateral attenuation equation (marked with a light solid line and labeled "Tail-LA" in Figure 15). In Figure 15, the SAE-AIR-1751 ground effects term has been scaled to be $-10.59e^{(-0.13\theta)}$. This scaling, when combined with the tail-mounted engine installation term, provides the same magnitude of lateral attenuation as SAE-AIR-1751 at an elevation angle of zero degrees.

4.7.3 Wing-mounted Engine Installation Algorithm

The wing-mounted engine installation results of the least squared empirical fitting to $Ae^{-0.13\theta} + C\theta + D$ are shown in Figure 15 as a dashed-and-dotted line labeled "Wing-only-EI;" the values of the coefficients are given in Table 9 below. For the wing-mounted engines, the Wallops engine installation data shows no effect above 20 degrees. The combination of the wing-mounted engine installation and the SAE-AIR-1751 ground effects term is shown as the dashed line labeled "Wing-LA". The underlying assumption in these new algorithms is that ground effects are independent of the type and location of the engines.

Table 9. Empirical Coefficients in Engine Installation Equation

Coefficient	Tail-mounted Engines	Wing-mounted Engines
A	-0.63673	-2.1266
C	0.035093	0.004388
D	-2.6345	-0.04119

4.7.4 Engine Installation Algorithm for propeller-driven airplanes

The data collected at Wallops do not show evidence of an engine installation effect for propeller-driven airplanes. However, noise from propeller-driven aircraft is still subject to ground effects. The ground effect component of lateral attenuation applies to all aircraft, regardless of engine type. It is assumed that the 1751 ground-to-ground algorithm is a reasonable approximation for propeller-driven aircraft. If the simplified SAE-AIR-1751 version of the ground effects is used, then the lateral attenuation for propeller aircraft is $-10.59e^{(-0.13\theta)}$. See Section 5 for more complete recommendations.

[iv] The sign of the equation has been switched from that found in SAE-AIR-1751 to conform to the convention used in this study.
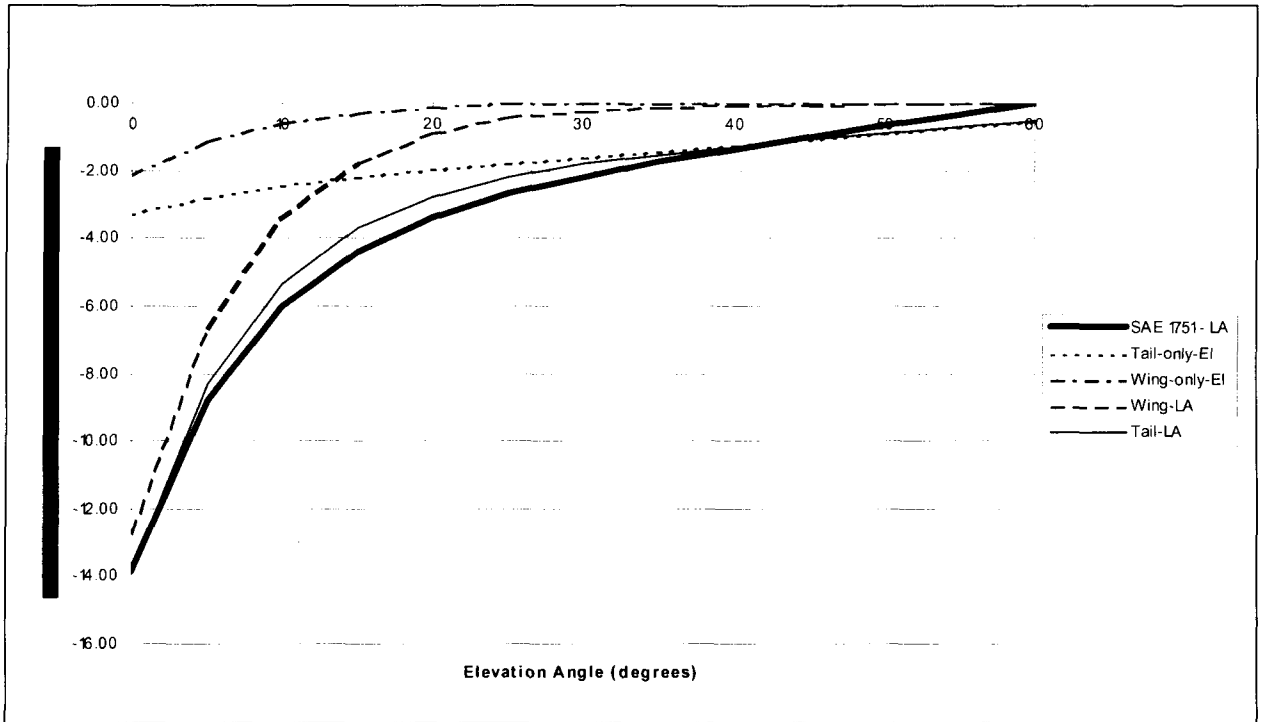
Figure 15. Wing- and tail-mounted lateral attenuation

5   Conclusion and Recommendations

Based on the analysis of the data collected at Wallops, the following conclusions are made:

- The data appear to support dividing the engine installation component of a new lateral attenuation algorithm into at least two equations, one for jet airplanes with wing-mounted engines, the other for jet airplanes with tail-mounted engines.

- Lateral attenuation / installation effects for the airplanes with tail-mounted engines substantially agree with SAE-AIR-1751.

- Lateral attenuation / installation effects for the airplanes with wing-mounted engines do not agree with SAE-AIR-1751.

- In agreement with SAE-AIR-1751, the Wallops data do not support an engine installation effect component of lateral attenuation for propeller-driven airplanes.

To support future enhancements to noise models, the current lateral attenuation algorithms should be split into engine installation and ground effects components. The engine installation component of lateral attenuation should be further divided into separate algorithms for airplanes with tail- and wing-mounted engines. The following engine installation algorithm is proposed for airplanes with the coefficients for the different airplane types listed in Table 10:

$$\text{Engine Installation Effect} = Ae^{-0.13\theta} + C\theta + D$$

Table 10. Engine Installation Effect Coefficients

Coefficient	Tail-mounted Engines	Wing-mounted Engines
A	-0.63673	-2.1266
C	0.035093	0.004388
D	-2.6345	-0.04119

The engine installation algorithms can be combined with the implicit ground effect term in the SAE-AIR-1751 lateral attenuation algorithm to yield the following new lateral attenuation equations (using the same parameters listed above for airplanes with wing- and tail-mounted engines):

$$\text{Lateral Attenuation} = \text{Ground Effect} + \text{Engine Installation Effect} = -10.59e^{(-0.13\theta)} + Ae^{-0.13\theta} + C\theta + D$$

It is recommended that the above equation replace the SAE-AIR-1751 long-range air-to-ground lateral attenuation equation in existing models. In the future, the two ground effects terms in SAE-AIR-1751 (the Overground and the Transition Region equations) can be replaced with aircraft specific ground effects. As is customary with new methodologies for aircraft noise modeling and assessment, such an update would need to be investigated and approved by the SAE A-21 Aircraft Noise Committee.

References

1. Society of Automotive Engineers, Committee A-21, Aircraft Noise. "Prediction Method for Lateral Attenuation of Airplane Noise During Takeoff and Landing," Aerospace Information Report No. 1751, Society of Automotive Engineers, Inc., Warrendale, Pennsylvania, March 1981.

2. Willshire, W.L. "Lateral Attenuation of High-By-Pass Ratio Engine Aircraft Noise," NASA Technical Memorandum 81968, National Aeronautics and Space Administration, Hampton, Virginia, April 1981.

3. Speakman, J.D., Berry, B.F., Modeling Lateral Attenuation of Aircraft Flight Noise, Internoise 92 Conference Proceeding, Toronto, Ontario, Canada: Internoise 92, July 1992.

4. Engineering Science Data Unit (ESDU) "Lateral Attenuation Calculations," ESDU AN66, London, England: ESDU, April 1990.

5. Bishop, D.E., Beckmann, J.M., Study of Excess Sound Attenuation as Determined From FAR Part 36 Aircraft Noise Certification Measurements, BBN Report No. 4219, Cambridge, MA: Bolt Beranek and Newman, May 1980.

6. Smith, M.J.T, et al., Development of an Improved Lateral Attenuation Adjustment for the UK Aircraft Noise Contour Model, ANCON, DRAFT, Environmental Research & Consultancy, Civil Aviation Authority, London, February 2002.

7. Storeheier, S.Å., et al., "Aircraft Noise Measurements at Gardermoen Airport, 2001," STF40 A02032, SINTEF Telecom and Informatics, June 2002.

8. Olmstead, J.R., et. al., Integrated Noise Model (INM) Version 6.0 Technical Manual, Report No. FAA-AEE-02-01, Washington, D.C., Federal Aviation Administration, 2002.

9. Ingard, K.U., "A review of the influence of meteorological conditions on sound propagation," J. Acoust. Soc. Am. Vol. 25, No. 3, pp 405-411, 1953.

10. Delaney, M.E., Bazley, E.N., "Acoustical properties of fibrous absorbent materials," Appl. Acoust. Vol 3, pp. 105-116, 1970.

11. Chessell, C.I., "Propagation of noise along a finite impedance boundary," J. Acoust. Soc. Am. Vol. 62, pp 825-834, 1977.

12. Fleming, G.G., et al., "A differential global positioning system for determining time space position information in support of aircraft noise certification," Proc.2001 National Technical Mtg., Inst. of Navigation, 2001.

13. Crighton, D.G., "Airframe Noise," Aeroacoustics of Flight Vehicles, ed. By H.H. Hubbard, ASA Press, 1995

14. Senzig, D.A., Fleming, G.G., Clarke, J-P.B., Lateral attenuation of aircraft sound levels over an acoustically hard water surface: Logan airport study, National Aeronautics and Space Administration CR-2000-210127, May 2000.

15. Embleton, T.F.W., Piercy, J.E., Daigle, G.A., "Effective flow resistivity of ground surfaces determined by acoustical measurements," J. Acoust. Soc. Am., Vol 74, No. 4, pp 1239-1243, October 1983.

16. Hodge, C.G., "Quiet Aircraft Design and Operational Characteristics," ibid, pp. 383-414.

17. Shams, Q.A., et al., Field-deployable Acoustic Digital Systems for Noise Measurements, International Military Noise Conference, Baltimore, Maryland, April 24-26, 2001.

R-2

18. Preisser, J.S. & Chestnutt, D. "Flight Effect on Fan Noise with Static and Wind Tunnel Comparison," J. Aircraft, Vol. 21, No. 7, pp 452-461, July 1984.

19. Lucas, M.J. and Marcolini, M.A. "Rotorcraft Noise Model," Proceedings of the American Helicopter Society Technical Specialists. Meeting for Rotorcraft Acoustics and Aerodynamics. Williamsburg, VA October 1997.

20. Gray, D.L., Wright, K.D., and Rowland, W.D., "A Field Deployable Digital Acoustic Measurement System," Proceedings of the NASA Technology 2000 conference, Washington D.C.

21. Wright, K.D., Martinson, S., and Comeaux,.T., "A Remote Acquisition and Storage System," Proceedings of the 45th International Instrumentation Symposium, Albuquerque, N.M., May 1999.

22. Lighthill, M.J., "On Sound Generated Aerodynamically: I. General Theory," Proc. R. Soc. London. A 211, pp 564-587, 1952.

23. Lilley, G.M., "On The Noise From Jets," Noise mechanisms, AGARD-CP-131, PP 13.1-13.12, 1974.

24. Freund, J.B., and Fleischman, T.G., "Ray traces through unsteady jet turbulence," Intl. J. Aeroacoustics, Vol. 1, No. 1, pp 83-96, 2002.

Appendix A: Research Team

Volpe National Transportation systems Center, Measurement and Modeling Division:

Gregg G. Fleming

B.S., Electrical Engineering, University of Lowell, MA. Mr. Fleming is the chief of the Volpe Center's Measurement and Modeling Division. He was responsible for all aspects of the study.

Paul J. Gerbi

B.S., Electrical Engineering, University of Lowell, MA. Mr. Gerbi provided data-reduction programming support.

Cynthia S. Y. Lee

B.S., Electrical Engineering, Northeastern University, Boston, MA. Ms. Lee provided data collection support.

Amanda Rapoza

B.S., Acoustic Engineering, University of Hartford, CT. Ms. Rapoza provided data analysis support.

David R. Read

Mr. Read was responsible for operating the video tracking system, both preparatory and in the field.

Judith L. Rochat

Ph.D., Acoustics, Pennsylvania State University, College Park, PA. Ms. Rochat provided support for operating the video tracking system.

Christopher J. Roof

B.S., Electrical Engineering and Music, Boston University, MA. Mr. Roof was a co-principal investigator on the study. He was involved with all aspects related to study design, data collection, data reduction and analysis.

David A. Senzig

M.S., Mechanical Engineering, University of Washington, Seattle, WA. Mr. Senzig was a co-principal investigator on the study. He was involved with all aspects related to study design, data collection, data reduction and analysis.

National Aeronautics and Space Administration (Langley)

Kevin P. Shepherd

Ph.D., Institute of Sound and Vibration Research, Southampton, U.K. Dr. Shepherd assisted with study design, acquisition of aircraft, and data analysis and interpretation.

David A. McCurdy

B.S., Aerospace Engineering, Auburn University, AL. Mr. McCurdy organized Langley's contributions to the study, coordinated the participating organizations, and oversaw the flight test safety review process.

National Aeronautics and Space Administration (Wallops)

Elizabeth L. West

B.S., Biology, Salisbury State University, Salisbury, Maryland. Ms. West was responsible for coordinating all Wallops Flight Facility assets in support of the study.

Civil Aviation Authority (England)

Sam White

B.Eng., Engineering Acoustics and Vibration, University of Southampton, England. Mr. White provided support for the video tracking system.

Wyle Laboratories

R. David Hilliard

B.S., Electrical Engineering, University of Tennessee, TN. Mr. Hilliard provided technical management and logistic support for the acoustic field operations.

Thomas G. Baxter

Acoustic Field Supervisor. Mr. Baxter was responsible for field operations associated with both acoustic data acquisition vans and the 200-foot vertical acoustic array.

Delta Air Lines

James Brooks

B.S., Mechanical Engineering, Auburn University. Coordinated test flight requirements between NASA and Delta Air Lines.

Private Consultant:

John-Paul B. Clarke

Ph.D., Aeronautics and Astronautics, Massachusetts Institute of Technology (MIT), Cambridge, MA. Professor Clarke assisted with study design and analysis.

Appendix B: Acoustic Instrumentation

This Appendix consists entirely of text and graphics taken directly from Reference 17.

Researchers at the National Aeronautics & Space Administration are engaged in acoustic research directed towards understanding and reducing noise generated by aerospace vehicles. The research involves numerous field test and measurements of noise signatures from various types of vehicles. Field measurement of noise radiated from flight vehicles provides information not available from wind tunnel tests. In the late 70's and early 80's, field measurements of aircraft noise (Ref 18) were used to verify theoretical predictions and to correlate with measurements made in wind tunnels. In the late 80's and early 90's, the increased emphasis on noise reduction technology for helicopters and tiltrotors (Ref 19), jet transporter, and future high speed transport placed strong demand for comprehensive field measurement systems. For over a decade, a Digital Acoustic Measurement System developed (Ref 20) at NASA Langley Research Center has been successfully used to make acoustic measurements with digitization at the microphones.

Figure 16 is a block diagram of the Digital Acoustic Measurement System (DAMS). The system consists of acquisition and recording systems. The acquisition system has four elements; The remote digitizers located at the microphone digitize the microphone analog outputs, the display and control subsystem, the encoder/decoder subsystem, and the digital acquisition-to-tape interface. Except microphones and remote digitizers, all the rest of elements are located in an instrumentation van that can be located up to 2000 feet away. The instrumentation vans are positioned at large distances from the microphones to reduce noise pickup from the van power generators and to avoid interference with the measurement. Digitizing the data at the microphone has allowed a significant increase in the dynamic range (30-40 dB) of the measurement, and this increased dynamic range has all but eliminated the need for operator gain changes normally required to maintain a good signal-to-noise ratio.
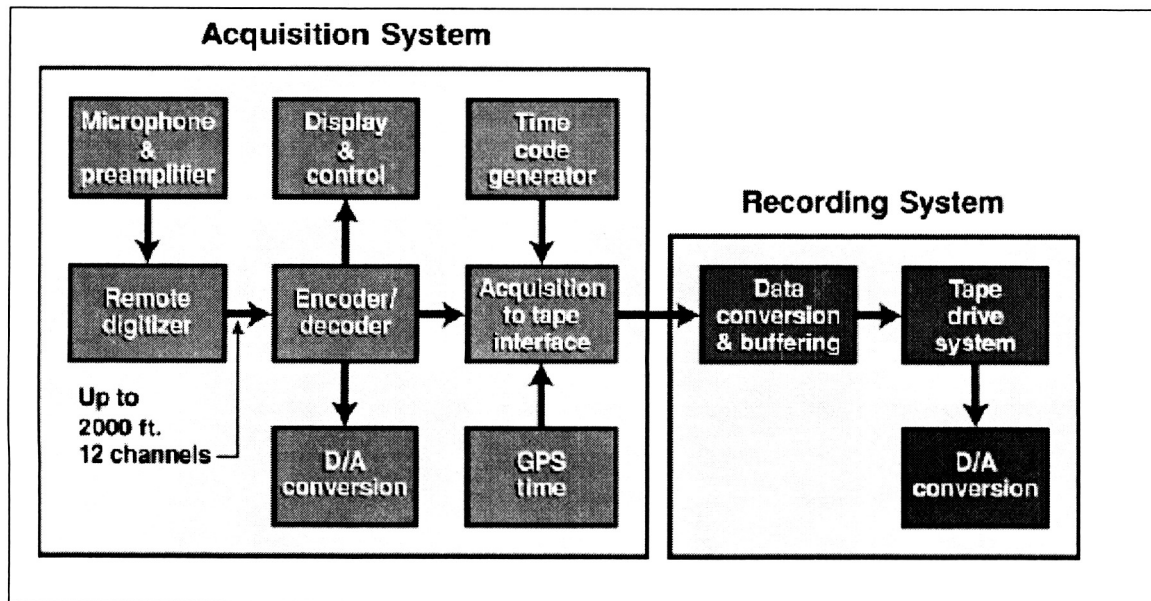

Figure 16. Digital Acoustic Measurement system

Acquisition System:
The acquisition system can be operated in either a synchronous mode or in a non-synchronous mode. In the synchronous mode, sample time is controlled from the instrumentation van; and in the non-synchronous mode, sample time is controlled by circuitry in each remote digitizer. The major elements of the acquisition system are the remote digitizers, the encode/decode subsystem, the display and control subsystem, and the digital-to-analog converter subsystem. Each of elements is discussed briefly as follows:

Remote Digitizer:
The remote digitizer is shown in block diagram form in Figure 17. This electronic system is powered by 6 volt

sealed lead acid batteries driving a DC-to-DC converter, which supplies several voltages to the electronics. The output of the microphone-preamplifier is input to a variable gain amplifier with gains of 1 to 128. The output of the microphone-preamplifier is low-pass filtered and sampled either in a synchronous mode or non-synchronous mode. The sampled analog data is converted to 16-bit digitized data by the analog-to-digital converter. The digital data is then converted to a serial data stream, encoded in a Manchester II code and transmitted to the instrumentation van.
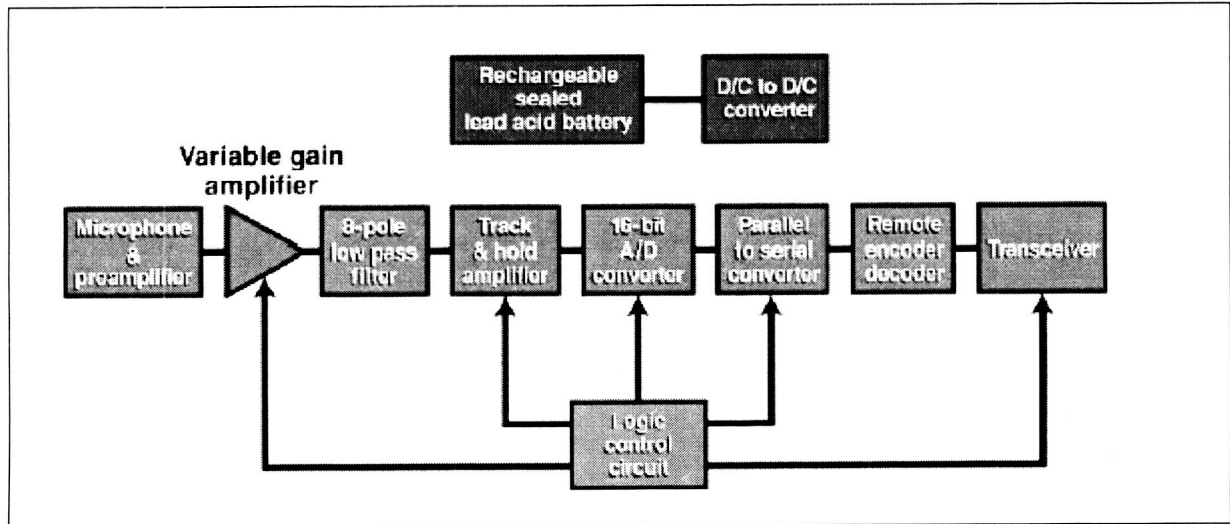
Figure 17. Remote DAMS Digitizer

Encode/ Decode System:
It is located in the instrumentation van. In the synchronous data mode, the system encodes the gains to be set on the variable gain amplifier and sends these gains to each remote digitizer, every time it is commanded to sample the microphone data. This system also decodes the Manchester coded data received from each remote digitizer. Full-duplex has been used for communication between the instrumentation van and the remote digitizer.

Display and Control System:
The display and control subsystem is used to display the amplitude of the data from each channel, set the gain of variable gain amplifier in the remote digitizer, detect and alert the operator of overload conditions, and of any faults in the communication of information and data between the instrumentation van and the remote digitizer. The display and control chassis is shown in Figure 18.
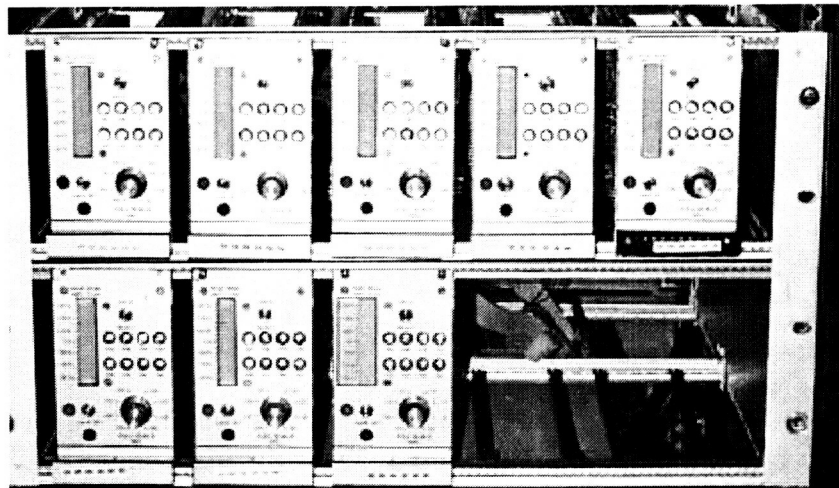

Figure 18. Display and Control Chassis

Digital-to-Analog Conversion System:
Each data channel has a digital-to-analog converter to allow the operator to monitor the data from each microphone. Converting the data to analog at several points in the serial path of the acquisition and recording system allows the operator to isolate system electronic problems to specific elements of the system.

Recording System:
Data from each microphone is filtered, sampled, digitized, and sent to a remote van. The received digitized data is collected and stored on a removable Jaz disk as shown in Figure 19 by a Data Acquisition System (DAS). The DAS consists of an embedded National Instrument PC running LabVIEW, and is stored on a removable Jaz disk. For several years, DAMS has been successfully used to make acoustic measurements with digitization at the microphone sites. However, the practical length of cables used to carry the digitized information to the instrument van where the data is stored on Jaz drive limits the size of the microphone array.
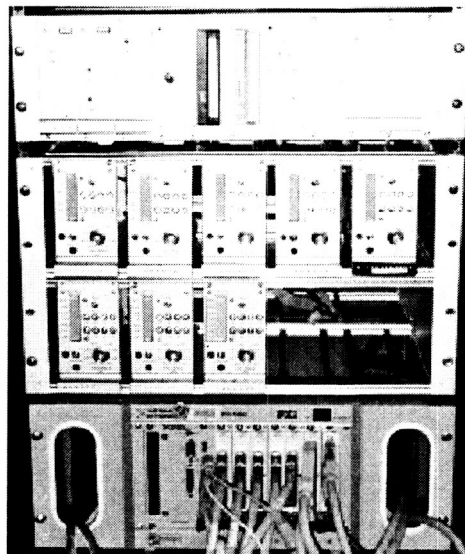

Figure 19. Jaz Drive and DAS

Appendix C: Video Tracking System

This appendix describes how to set–up the video tracking equipment. Equipment used in the test is described when introduced. This set-up was used in the Wallops test.

<u>System Calibration:</u>

Prior to beginning field measurements, the system was calibrated. System calibration included determining the relationship between the pixel representation of a given image and the actual azimuth and elevation angles of that image from the center of the camera. The method of determining this relationship is described in this sub-section.

The system calibration was based on knowing both the pixel representation of a known object and the actual azimuth and elevation angles of that object in three-dimensional space. For this video system, the known object was an orthogonal grid projected onto a large screen (approximately 9 feet by 16 feet).

The heights above the ground of the upper and lower corners of the grid on the screen were measured. The origin point on the grid was arbitrarily chosen. A laser was attached to the camera so that the entire camera and laser assembly could be rotated and translated on the three-axis tripod head. The origin of the grid was illuminated with the laser so that the height of the camera above the ground could be adjusted to match the height of the grid origin above the ground. This height was noted and used in later calculations of azimuth and elevation.

With the camera and grid point positions known in three-dimensional space, a transformation of the pixels of the filmed grid to a spherical system centered on the camera was performed. Pixels not on the actual grid were found from linear interpolation. No extrapolation beyond the known grid was performed.

<u>Set-up of Camera and Optical Target locations:</u>
The user determines a Cartesian coordinate system to use during the test. Typically, this Cartesian coordinate system is defined separately from the video system by the geometry of the test site. For example, if a test aircraft will fly a known linear track, then that track can be defined as a primary axis (positive or negative X or Y). Or, if the test is being conducted in conjunction with acoustic measurements, the microphone array may define the primary axes. For the Wallops test, the runway centerline was used as the X axis (positive to the east) and the microphone array as the Y axis (positive to the north), with the Z axis being positive up.

The cameras are manually located where both cameras can observe and record the motion of the object of interest. The cameras should be placed so that the separation of the cameras is approximately the same distance as the distance from the cameras to the object. Optical Targets are manually placed in the field of view of the cameras. Each camera must have two targets in its field of view during the entire event of interest. The cameras can be rotated between events of interests as long as the optical targets remain in view. For the Wallops test, the cameras were located approximately 600 feet to the south of the runway centerline, with one camera sub-system 250 feet to the west and the other 250 feet to the east of an extended line through the microphone array.

The Optical Targets are designed to mount on top of standard consumer-grade photography tripods. When mounted, the Optical Targets should be two to three ft. above the ground. The Direct Targets should be placed 60.0 ft. from their associated cameras along a line from the cameras to the point where the greatest accuracy of the object's position is desired. The Angle Targets should be placed 30.0 ft. away from the Direct Targets on a perpendicular line. This camera/target geometry forms a right triangle that has a hypotenuse of 67.08 ft. This hypotenuse is the distance from the cameras to their associated Angle Targets. These distances are not requirements; however, using these distances eases troubleshooting since the targets are designed to be easily visible at such distances and the use of right triangles simplifies any field calculations required for checking the geometry of the camera/target layout. Before placing the Optical Targets and cameras, stakes are driven into the ground at the locations noted above. These stakes should be marked with survey tape, or some other method, so that they can easily be found later when the Targets and Cameras are removed at the end of the measurement program.

The location of the cameras and optical targets are noted and logged for later use by the system software. The cameras and optical targets can be accurately located with the use of a dGPS system (see Reference 12) and

conventional survey equipment. Field usage of the Volpe dGPS system has shown satisfactory accuracy (within 20 cm) in the horizontal plane of the measurements, but vertical measurements have required more accuracy than the dGPS typically provides. For the vertical measurements, conventional survey equipment is used.

The cameras and Optical Targets should now be mounted on their tripods and placed directly over the survey locations. For the Optical Targets, this means placing the center of each target over the associated survey point and rotating the target so that the black-and-white side faces the camera. For the cameras, this means placing each camera so that the center of the wide angle lens/camera attachment point is directly over the associated survey point. For each target and camera, the height of the center point above the associated survey point should be noted on the Log Sheet.

The Optical Target tripods should be staked down. Unless this is done, the targets will blow over in the slightest breeze. An efficient way to do this is to hammer a stake into the ground at each of the tripod's ft. and use a plastic zip-tie to firmly attach each foot to a stake.

Each camera sub-system includes an LED box and mounting hardware. The use of the LED box is described below. To assemble the sub-system, first attach the tripod's removable mounting plate to the LED mounting arm using the counter-sunk ¼ inch machine screw found in the camera kit. Then, mount the arm to the camera uses the existing tripod mounting ¼ inch threaded hole in the bottom of the camera. Snap the assembled camera and LED to the tripod, using the tripod's removable mounting plate to secure the entire camera sub-system. Finally, connect the 2.5 millimeter LANC controller to the LANC port on the camera and connect the BNC connector to the LED box. Extend and connect the LANC and LED cables to the RM-95 controllers and the 705, respectively.

Camera Power:
Each camera has a DC power converter (Canon part number CB-900) in the associated carrying case. This power converter has a "cigarette lighter" plug terminal. Each carrying case is equipped with a cigarette lighter receptacle with battery clips on the opposite end of the cable. When connecting the battery clips to the battery, note which clip is positive and which is negative. Incorrect polarity applied to the camera system will destroy the DC power converter. The Canon DC-900 DC coupler will attach into the CB-900 and supply power to the camera.

Turn the camera on by sliding forward the power switch on the left side, then move the lever on the front right corner of the camera from "LOCK" to "MOVIE." The red LED on the power switch illuminates and either the LCD monitor or view-finder activates and begins reporting the camera status. The user can toggle between the view-finder and the LCD monitor depending on preference by pressing the MONITOR/FINDER button on the upper left side of the camera. Remove the lens cap and make sure the optical targets are in the field of view.

Tape Installation:
Before installing a new tape in the camera, the test information should be physically written in indelible ink on the outside of the tape cassette. This test information should include the date of the test, the camera system number, and the tape number (if more than one tape is used per camera). Writing this information on the cassette box is not adequate, as boxes and tapes are often interchanged.

The user installs the tapes by lifting up the side latch on the tape door and rotating the tape door forward on the camera. The tape is installed TGIF ("Tape Goes In First") into the tape transport mechanism. Gently press down on the tab that says "CLOSE THIS FIRST." At this point, the camera detects the presence of the tape and moves the tape into position for recording. During this movement, several steel and nylon gears can be seen rotating near the tape door. These gears are adjusting the tape tension. *Do not close the tape door until all motion of these tensioning gears stop.* If the camera is still moving the tape or if the tensioning gears are still working, the camera will deliver an error message stating that the tape must be removed and reloaded. When all gear motion ceases, wait several seconds, then close the tape door. If the tape is properly loaded, no error message will be seen.

Camera Set-up:
Once power is installed, the camera's internal clock can be checked and updated if needed. This internal clock is not used for camera coordination, but an accurate internal clock eases post-processing since this clock information is written directly onto the digital tape and can be used to quickly find events that occurred at a known time.

The camera should be set to Progressive scan mode, with a fixed aperture of f22, and Optical Image Stabilization turned off. In addition, the focus should be set at infinite and then the auto-focus feature should be turned off. Each of these procedures is described in detail in the Optura Instruction Manual included in each camera system carrying case.

When the camera set-up is complete, the camera menu should contain the following settings:

```
D.ZOOM          OFF
WIND SCREEN     AUTO
WHITE BAL       AUTO
16:9            OFF
MOVIE MODE      PRO.SCAN
SENSOR          ON
TALLY LAMP      OFF
AUDIO MODE      16bit
REC MODE        SP
D/TIME SET      As required
```

In addition to the camera set-up, the tracking system requires the setting up of the time coordination sub-system. The time coordinate sub-system is comprised of a True Time 705 GPS-based time code generator (705), a laptop computer with a confirmed working copy of the Volpe-written "truetime.exe" software, an RM-95 camera controller, LED boxes, and LED boxes mounting hardware. The 705 should be connected to its power supply and its antenna. After these are connected, the 705 should be connected to COM port 1 on the laptop computer via the serial cable. The SMB connector on the front of the 705 should be connected to the cable(s) that lead to the LED box in front of the cameras. The SMB connector is routed through a T-connector so that both LED box fire based on one signal from the 705. Finally, the RM-95s should be connected to each camera's LANC port. Each of these pieces of sub-system equipment, with the exception of the LED boxes (which are mounted directly on the camera), should rest on a table within easy reach of the user. The 705 can now be turned on.

Activating the Cameras:
The Optura video cameras will enter an inactive state ("sleep") if they remain in "pause" mode for more than five minutes. The user can re-activate ("wake") the cameras by pressing the green button on the RM-95 labeled "POWER." Note that no instruction manual exists for the RM-95. Both cameras should be woken at the same time. The RM-95 will indicate that the camera is working correctly by reporting the tape location in minutes and seconds (not frames). Below the time display, the RM-95 should show a round dot, ●, next to two vertical parallel lines, ‖. The round dot indicates that the Optura is in camera mode (as opposed to VCR mode); the parallel lines indicate that the camera is in pause mode (as opposed to recording).

Starting and Stopping Recording:
Recording can be started and stopped by pressing the red START/STOP button on the top right corner of the RM-95. When the camera is running, the running time code is displayed on the RM-95. When the camera is paused, the time code is static and the pause mode symbol is displayed.

Data collection:
Before the beginning of data collection for an event of interest, the cameras are turned on and the "truetime.exe" program is used to tell the 705 to generate a signal (a TTL signal on the SBC connector) at a known time for a known duration for recording on the camera's media. This signal is used for coordinating the timing of the cameras. The time and duration that this signal is sent to the cameras is automatically recorded in a computer file generated by "truetime.exe".

After the reception of the timing signal, the cameras continue to run until the operator manually turns the cameras off. The system allows multiple events of interest to be collected after a timing signal has been received. This allows the cameras to be coordinated, then left to run until the end of the recording medium is reached. Conversely, the cameras can be stopped and started for each event of interest, so long as a timing signal is acquired each time the cameras are restarted. At Wallops, the cameras were stopped at the end of each event and re-started at the beginning of the next.

If the cameras run for an extended period of time, a second time signal can be sent to the cameras at the end of the event of interest so that any drift in timing of the cameras can be logged and accounted for in the processing of the recorded data.

Post-Processing:
After the tracking data were collected in the field, these data were converted into a form usable by the Volpe Center's video data reduction computer programs. These computer programs are described in the following sub-sections.

Video Data Reduction - Preprocessing and Tracking Programs
The translation of an aircraft event from the X-Y pixel system and local time recorded by the cameras to the measurement time and coordinate systems used by the other processing programs involved several steps. One set of steps dealt with the time transforms, the other dealt with the coordinate transforms.

The time transform involved four steps. The first step was the calculation of the difference between the camera time and UTC time of the coordination signal on the LED box at the beginning (or ending) of the recording. The second step was the calculation of the expected camera time at the end (or beginning) of the recording using the NTSC drop code time frame system[*]. If the expected camera end time did not match the reported camera end time, then a camera time drift occurred. The third step applied a linear approximation of any drift to all times on the tape. The fourth step was to use the NTSC drop code time frame system to exactly match the drift-corrected camera time with UTC time. In the Wallops measurement program, the video cameras were turned on and off at the beginning and ending of each pass. These passes were generally a minute or less in duration. For these short times, camera drift is not an issue, so steps two and three were by-passed.

The coordinate transform involved five steps. The first step was to convert the X-Y pixels into the elevation and azimuth angles of a spherical coordinate system centered on the camera. This step made use of the grid interpolation process discussed above. The next step was to transform this spherical system to a normalized Cartesian system. This Cartesian system was then rotated twice, first about the roll axis and then about the pitch axis. Next, the Cartesian system was re-translated back to a final spherical system. Finally, the azimuth angles of the final spherical system were used to find a vector from each of the cameras to the aircraft in the measurement program's XYZ coordinate. A line segment of minimum distance between the two vectors was determined. The aircraft position was taken to be at the midpoint of this line segment.

The output of the program was the three-dimensional aircraft position in the measurement coordinate system at one-second intervals. Also included in the output computer file were aircraft type information, data on the location of the microphones, and the ground surface impedance; these data were passed through the program without modification.

Each camera sub-system can track an object through approximately 60 degrees of arc. At Wallop, this translated to approximately 3 to 4 seconds of tracking time.

System Accuracy:
The video TSPI system was tested for accuracy on several occasions using the Volpe Center's dGPS TSPI system as a reference. In general, when compared with the dGPS, the video system was within 10 feet in each of the three axes while tracking airplanes at a slant distance of 500 feet at the point of closest approach.

---

[*]The NTSC system operates at 29.97 frames per second. For frame counting, each second is assumed to have 30 frames, except that the first second of every minute that is not evenly divisible by 10 contains only 28 frames.
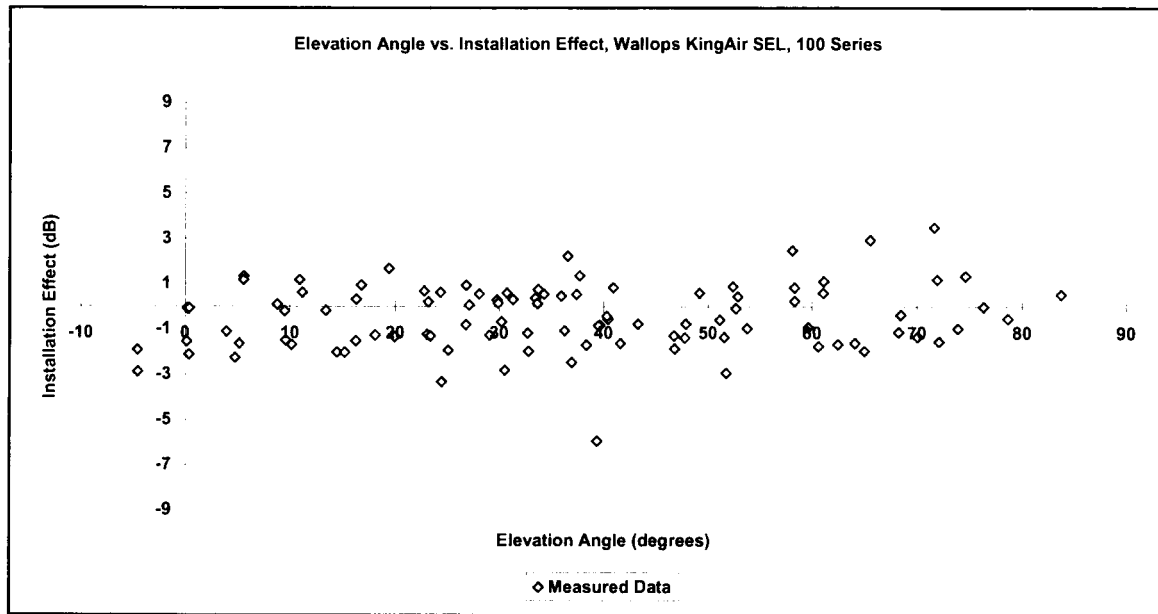
Appendix D: Data Graphics

Elevation Angle vs. Installation Effect, Wallops KingAir SEL, 100 Series

Figure 20. King Air Installation Effect, 100 Series Passes

Elevation Angle vs. Installation Effect, Wallops KingAir SEL, 200 Series
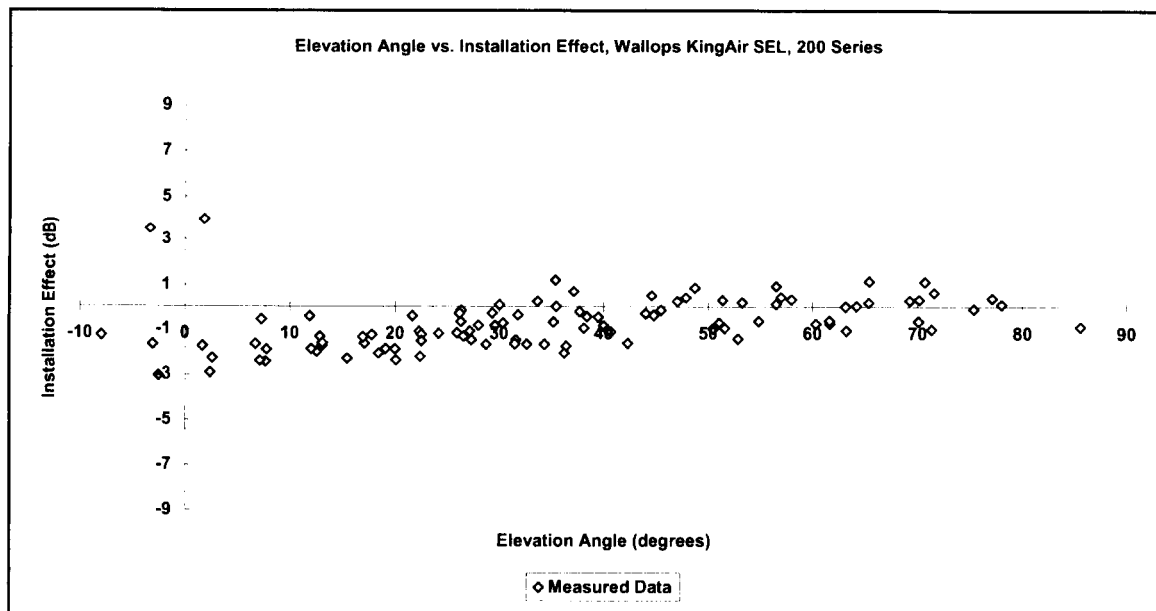
Figure 21. King Air Installation Effect, 200 Series Passes

Elevation Angle vs. Installation Effect, Wallops KingAir SEL, 300 Series
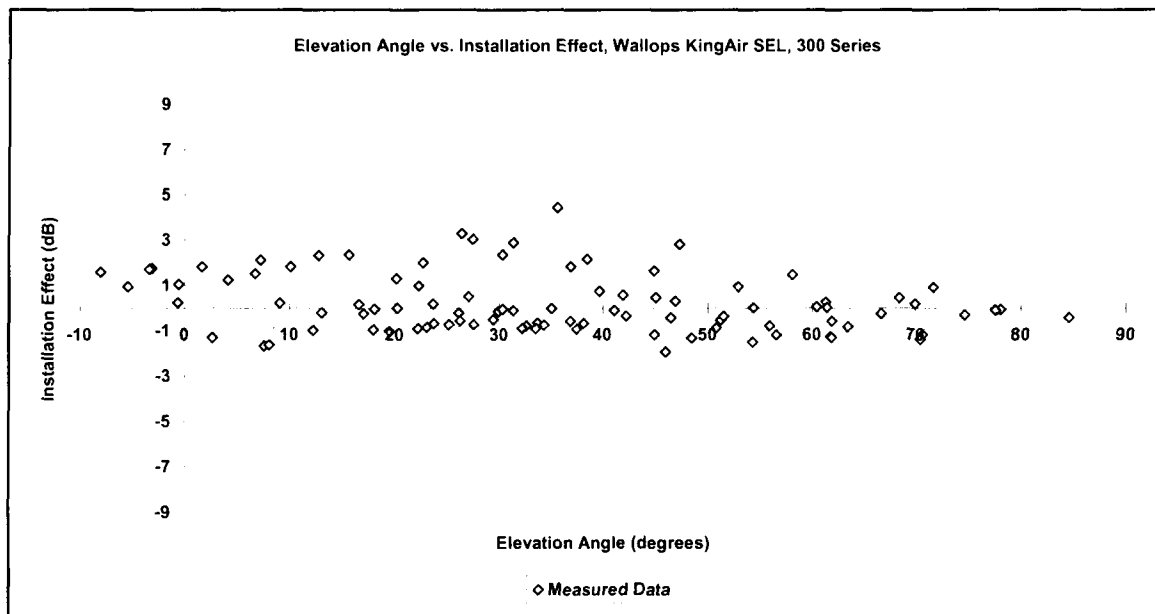
Figure 22. King Air Installation Effect, 300 Series Passes

Elevation Angle vs. Installation Effect, Wallops KingAir SEL, 400 Series
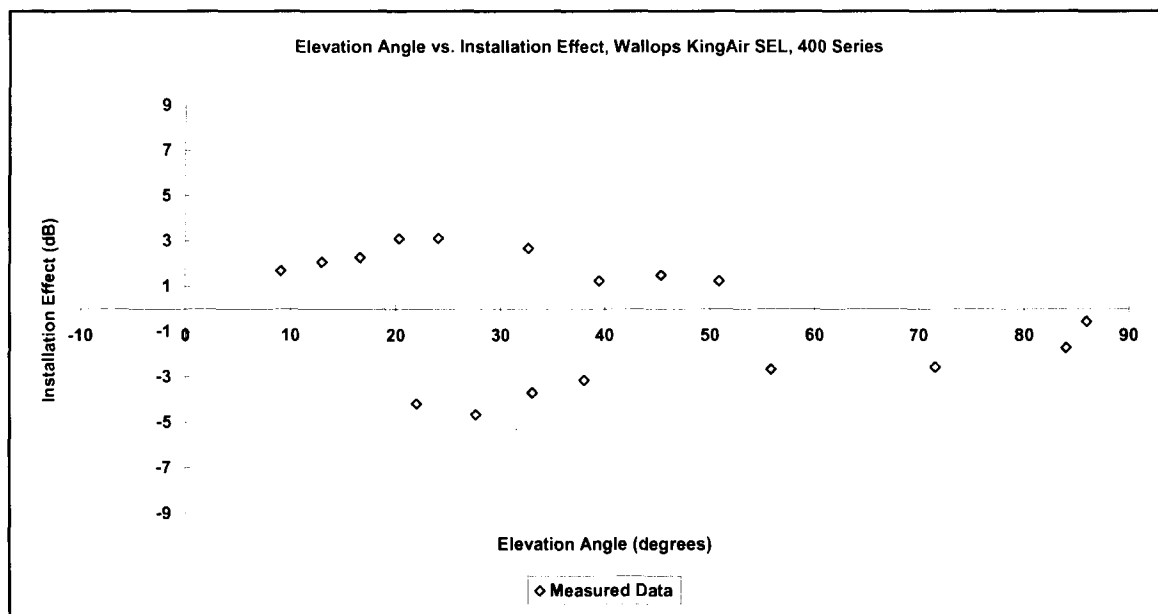
Figure 23. King Air Installation Effect, 400 Series Passes

Elevation Angle vs. Installation Effect, Wallops Falcon SEL, 100 Series
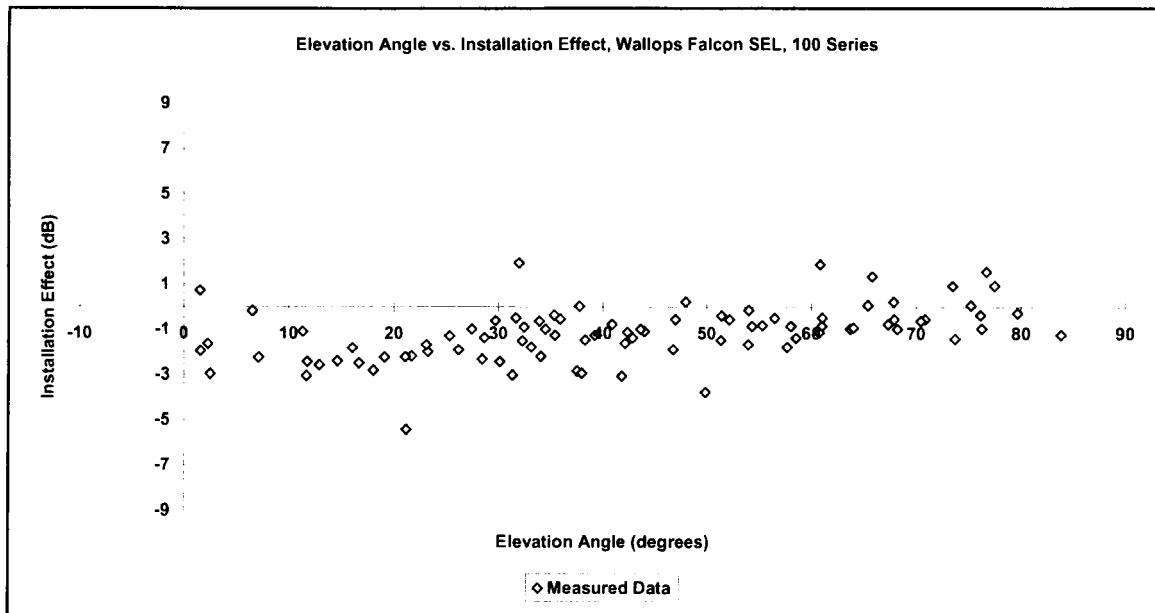
Figure 24. Falcon 2000 Installation Effect, 100 Series Passes

Elevation Angle vs. Installation Effect, Wallops Falcon SEL, 200 Series
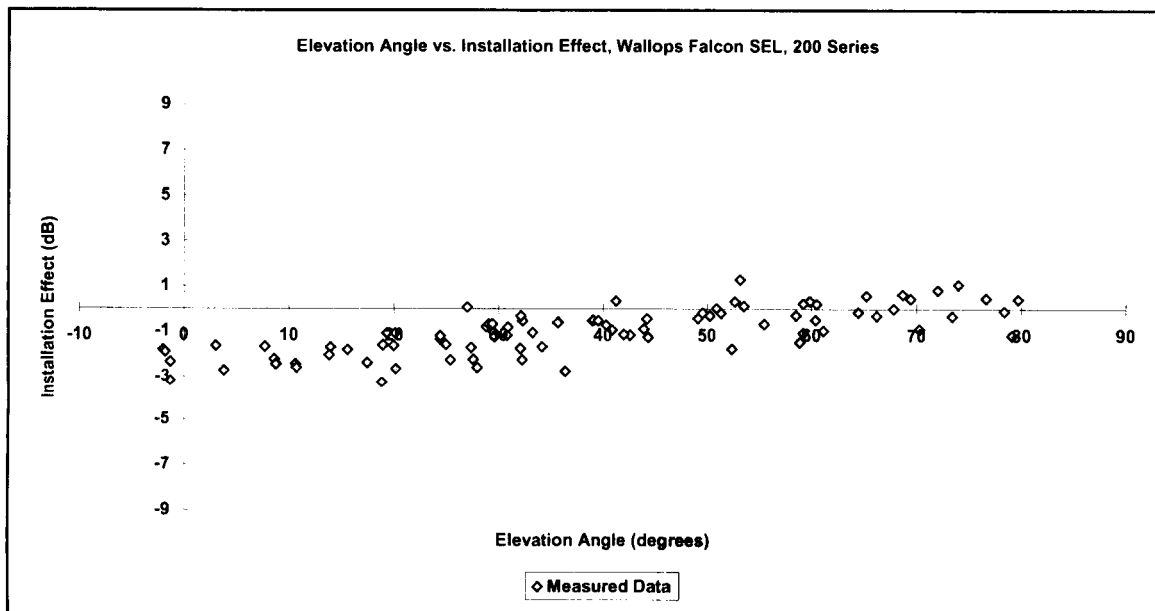
Figure 25. Falcon 2000 Installation Effect, 200 Series Passes

Elevation Angle vs. Installation Effect, Wallops Falcon SEL, 300 Series
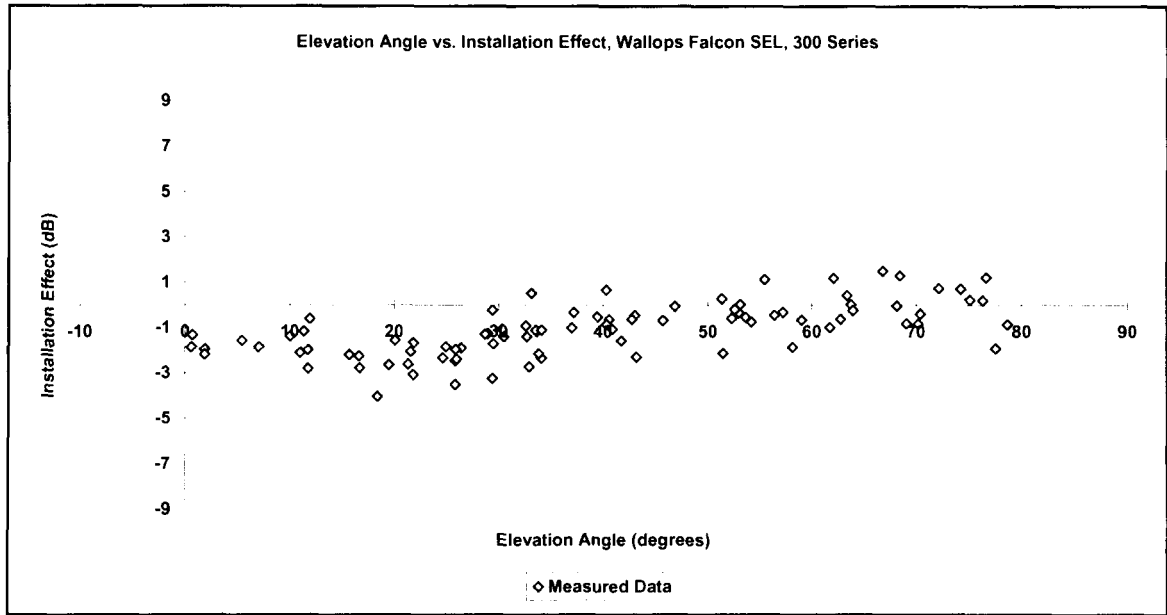
Figure 26. Falcon 2000 Installation Effect, 300 Series Passes

Elevation Angle vs. Installation Effect, Wallops Falcon SEL, 400 Series
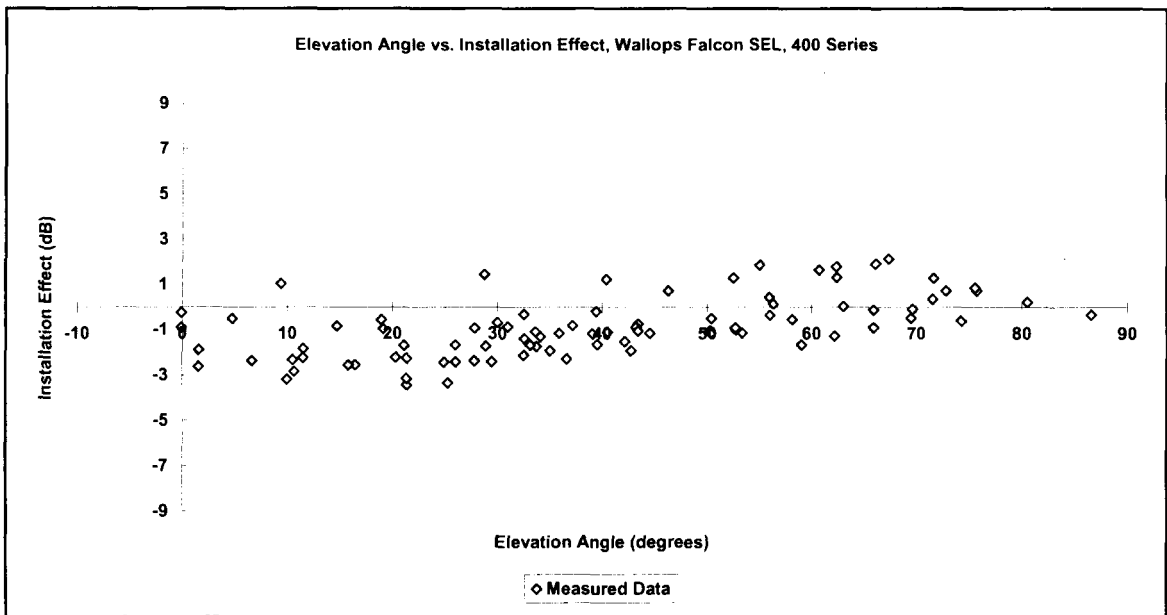
Figure 27. Falcon 2000 Installation Effect, 400 Series Passes
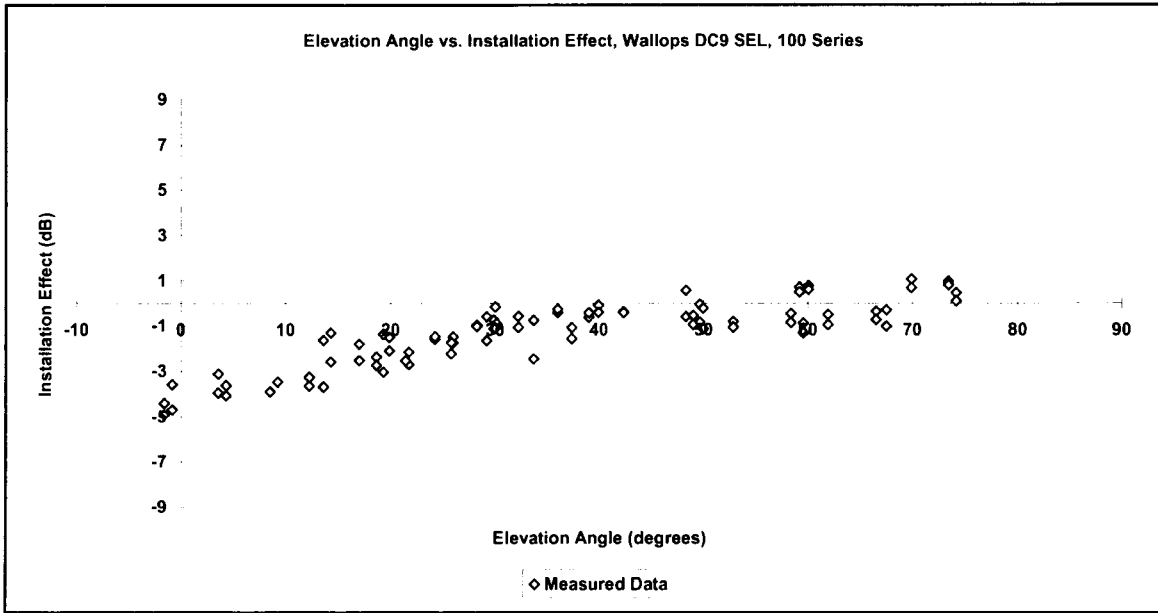
Figure 28. DC-9 Installation Effect, 100 Series Passes
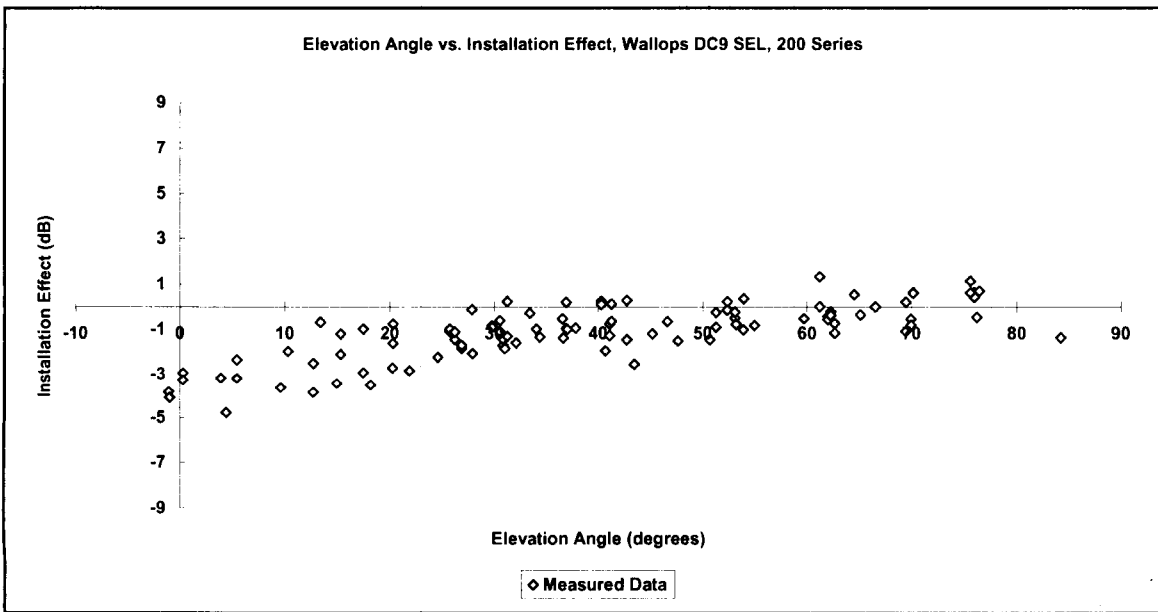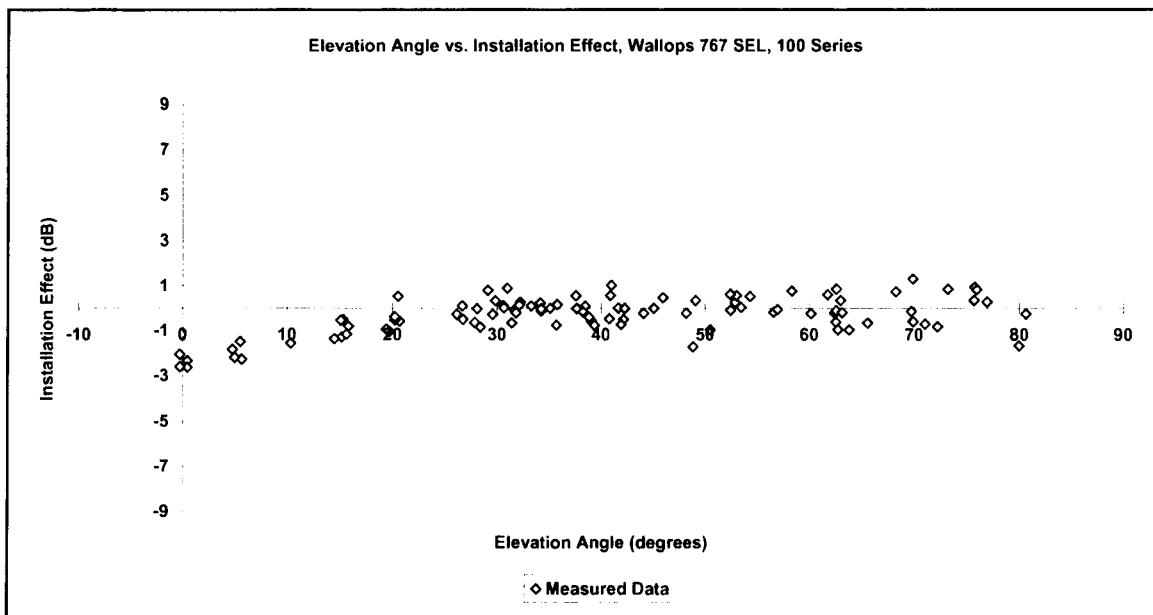

Figure 29. DC-9 Installation Effect, 200 Series Passes
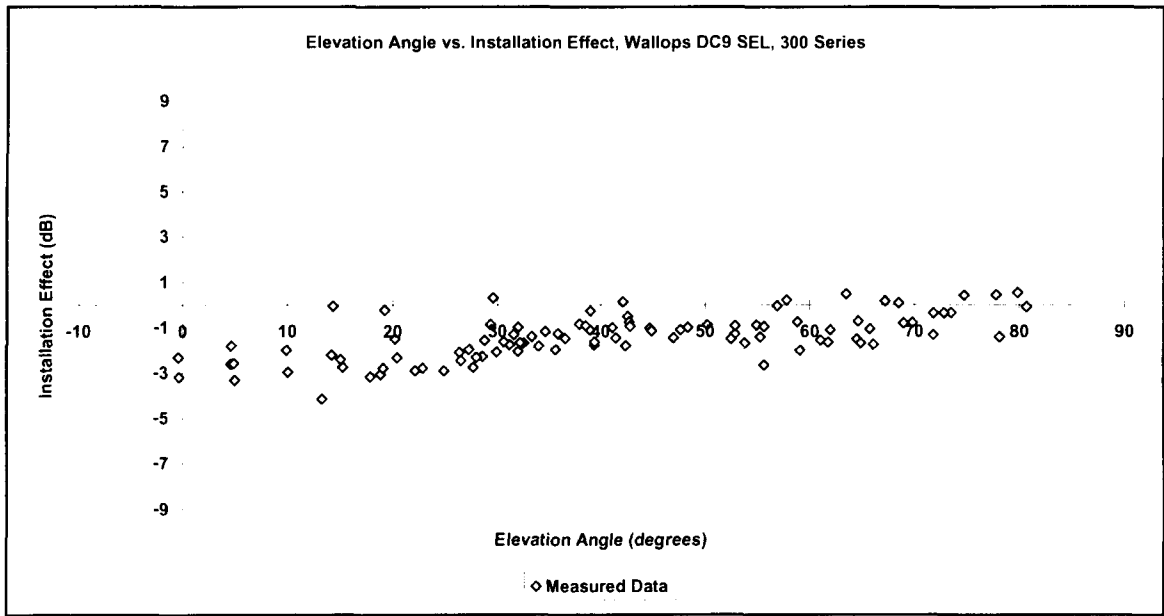
Figure 30. DC-9 Installation Effect, 300 Series Passes
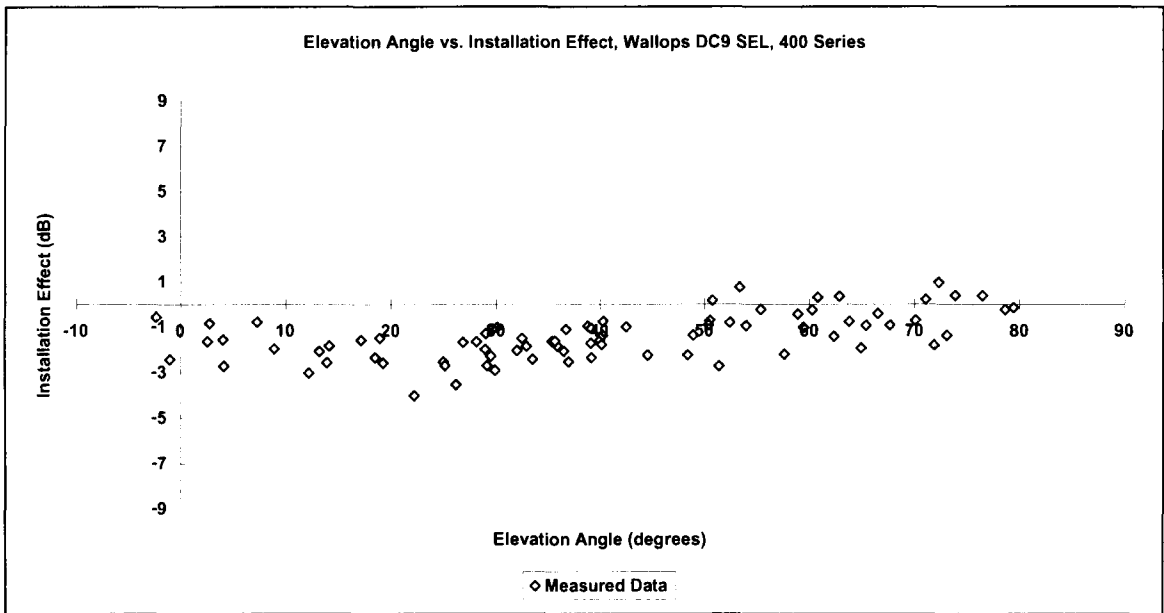
Figure 31. DC-9 Installation Effect, 400 Series Passes
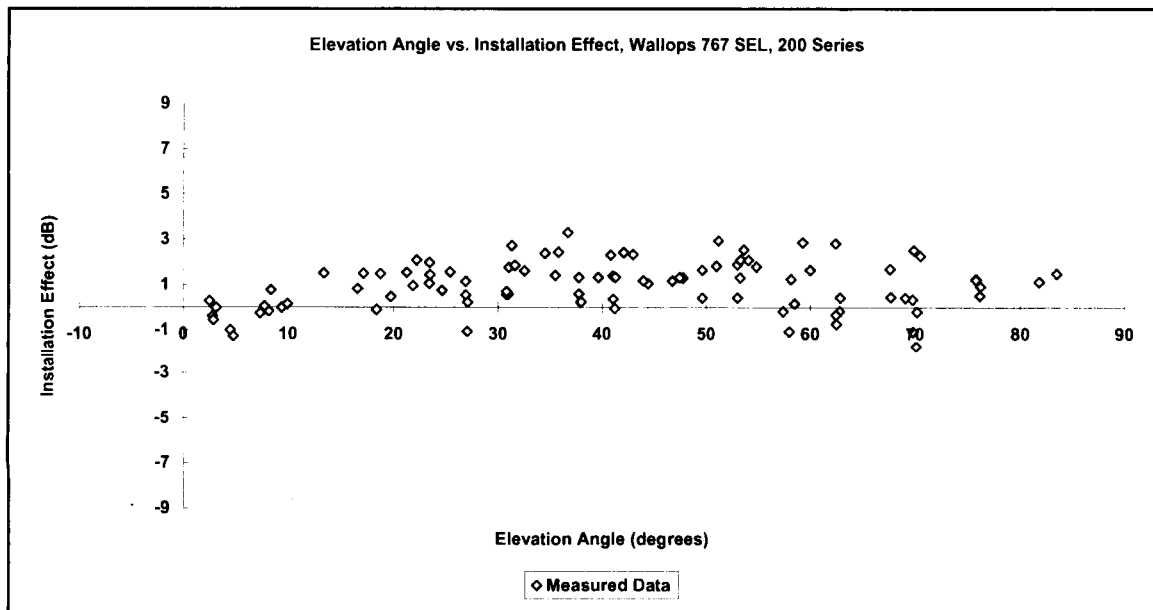
Figure 32. 767 Installation Effect, 100 Series Passes

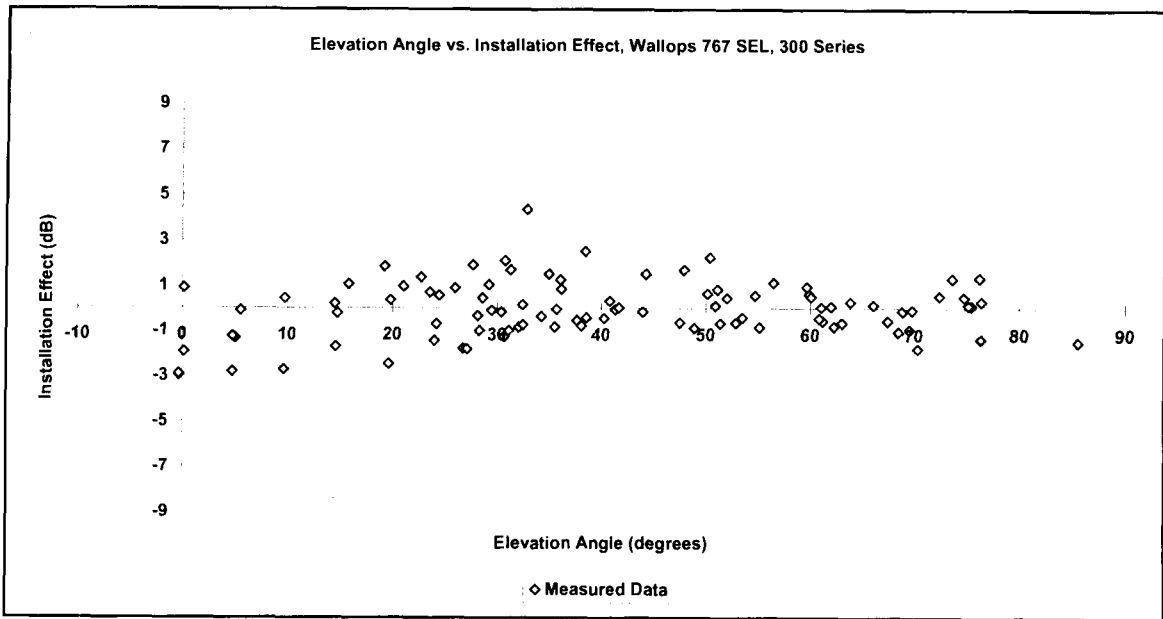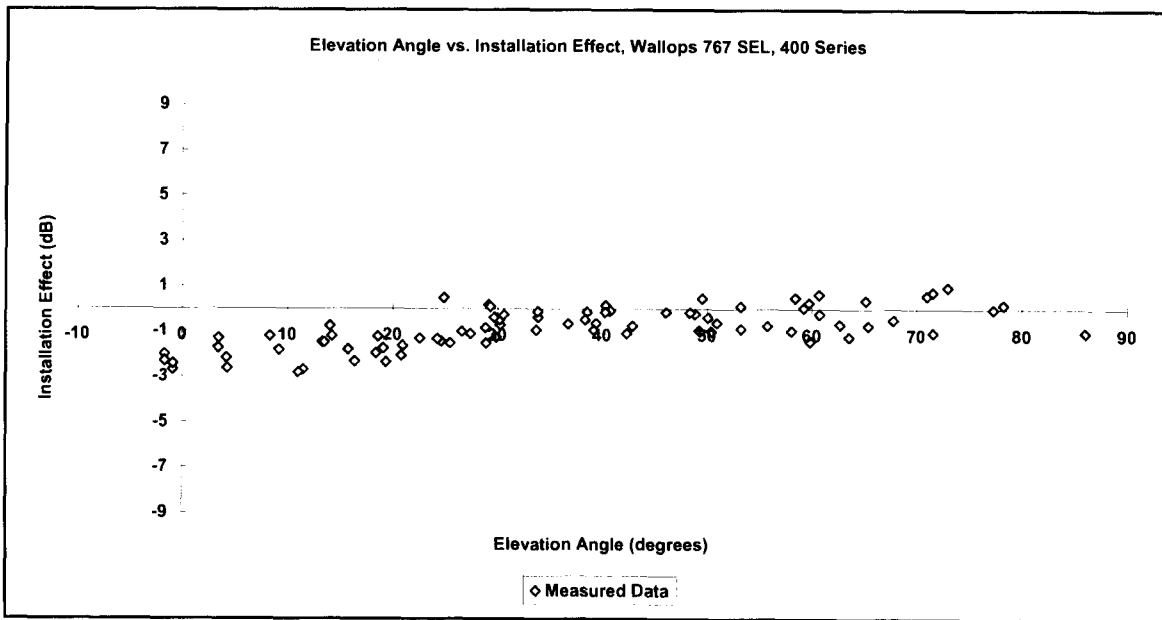

Figure 33. 767 Installation Effect, 200 Series Passes

Elevation Angle vs. Installation Effect, Wallops 767 SEL, 300 Series

Installation Effect (dB)

Elevation Angle (degrees)

◇ Measured Data

Figure 34. 767 Installation Effect, 300 Series Passes

Elevation Angle vs. Installation Effect, Wallops 767 SEL, 400 Series

Installation Effect (dB)

Elevation Angle (degrees)

◇ Measured Data

Figure 35. 767 Installation Effect, 400 Series Passes

Appendix E: Jet Shielding Model

This Appendix discusses a simplified model for examining the physical effects of jet shielding for a two-engine airplane. The model was developed to provide a mathematical expression for the data collected in this study. This model is not intended to be a rigorous exposition of jet noise. The reader is directed to the classic works of Lighthill (Ref. 22) and Lilley (Ref. 23), as well as more recent works (Ref. 24) for a first principles examination of jet noise.

The model depends on three physical parameters that the user can manipulate to match empirical data. Two of these physical parameters relate directly to the geometry of the engine and airframe combination. The third parameter relates to the strength of the jet's ability to block the noise of the opposite jet; this parameter accounts for the attenuation of sound traveling the acoustic path through the jet flow.

Figure 36 below shows an idealized schematic of the geometry of the airplane's engines, where the two circles represent the jet plumes. The reader's perspective is from the nose of the airplane. The parameter d represents the distance between the centers of the two engines' jet flows. The parameter R represents the radius of the jet plume. The variable θ represents the angle from the airplane to the ground observer; the stylized microphone in the figure. The other variables shown in Figure 36 are derived. L represents the distance of the sound path from the center of one engine's plume through the jet plume of the other engine. The l variable represents the perpendicular distance from the jet flow centerline to the acoustic path. The r variable represents the radial distance from the jet flow centerline to an arbitrary point along the acoustic path.
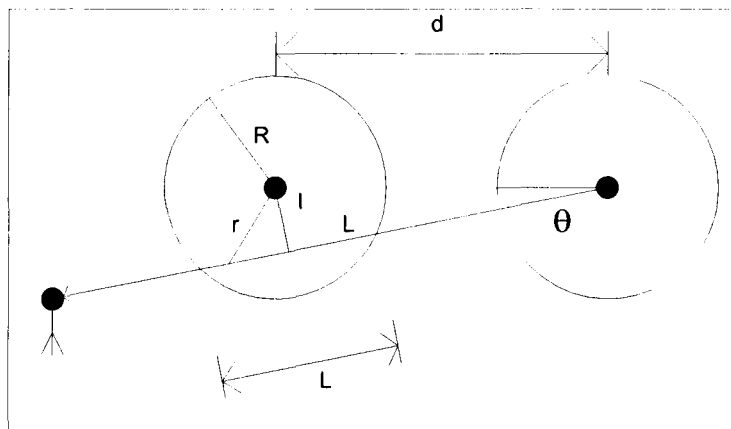

Figure 36. Geometry of Jet Shielding

The measure of the attenuation of the acoustic path through the jet flow is represented by the b parameter. In this simplified model, the attenuation is a linear function of the distance from the centerline of the engine. Figure 37 below shows a graphical representation of this relationship.
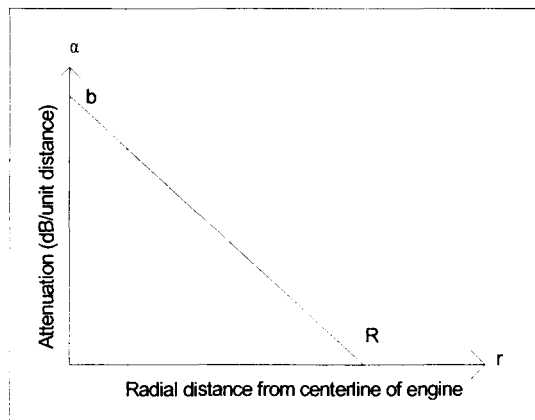

Figure 37. Relationship between radius and attenuation

The mathematical representation of the relationship shown in Figure 37 is

$$\alpha = \frac{-b}{R}r + b \qquad\qquad \text{Equation 1}$$

where α is the attenuation in dB/distance as a function of the radial distance r. The attenuation is a maximum of b at the center of the jet and decreases linearly to zero at the outer radius of the jet flow R.

Figure 38 shows a detail of the acoustic path through the jet flow first shown in Figure 36. The variable x is the distance along this path, so that Δx represents an incremental distance.
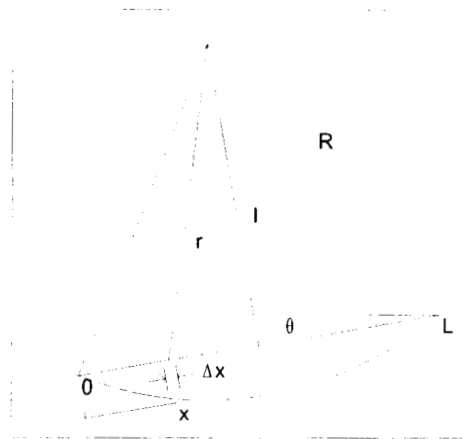

Figure 38. Detail of Acoustic path through Jet Flow

A number of geometric relationships exist for the given variables and parameters. The R, L, r, x, and l parameters and variables are related by the following equations:

$$l = d \sin \theta \qquad\qquad \text{Equation 2}$$

$$L = 2\sqrt{R^2 + l^2} \qquad\qquad \text{Equation 3}$$

$$r = \sqrt{l^2 + \left(\frac{L}{2} - x\right)^2} \qquad\qquad \text{Equation 4}$$

The attenuation through an incremental segment of the acoustic path is given by:

$$\Delta atten = \alpha \Delta x$$

$$\Delta atten = \left(\frac{-b}{R}r + b\right)\Delta x$$

$$\Delta atten = \left(\frac{-b}{R}\sqrt{l^2 + \left(\frac{L}{2-x}\right)^2} + b\right)\Delta x$$

Changing from incremental to infinitesimal notation and taking the integral of both sides:

$$atten = 2b \int_0^{L/2} \left(1 - \frac{1}{R} \sqrt{l^2 + \left(\frac{L}{2-x}\right)^2} + b \right) \delta x$$

$$atten = bL - \frac{2b}{R} \int_0^{L/2} \sqrt{l^2 + \left(\frac{L}{2-x}\right)^2} \, \delta x \qquad \text{Equation 5}$$

The general form of the integral on the right side of Equation 5 is:

$$\int \sqrt{a^2 + u^2} \, \delta u = \frac{u}{2}\sqrt{a^2 + u^2} + \frac{a^2}{2} \ln\left(u + \sqrt{a^2 + u^2} \right) + C$$

Using the substitution $g(x) = x - L/2 = u$ results in the following transformed equation:

$$atten = bL - \frac{2b}{R} \int_{-L/2}^0 \sqrt{l^2 + u^2} \, \delta u$$

$$atten = bL - \frac{2b}{R} \left(\frac{u}{2}\sqrt{l^2 + u^2} + \frac{l^2}{2} \ln\left(u + \sqrt{l^2 + u^2} \right) \right) \Bigg|_{-L/2}^0$$

The simplified form of the above equation is:

$$atten = b \left(\frac{L}{2} + \frac{l^2}{R} \ln\left(\frac{R - L/2}{l} \right) \right) \qquad \text{Equation 6}$$

Equation 6 represents the attenuation of the sound of the farther engine (*Engine₁*) as it passes through the jet flow of the closer engine (*Engine₂*). However, the noise heard by the receiver is a combination of sound from both engines. The sound from *Engine₁* is attenuated by the amounted given in Equation 6. The sound from *Engine₂* travels to the receiver without this attenuation. If the initial sound energies (*I*) of both engines are identical:

$$I_{Engine_2} = I_{Engine_1}$$

Because the sound from *Engine₂* is un-attenuated, the transmitted energy (*T*) is equal to the initial energy of either engine:

$$T_{Engine_2} = I_{Engine_2} = I_{Engine_1}$$

If the energy is given in terms of decibels, then the transmitted energy can be converted to a ratio of energies and then can be summed:

$$Transmitted\ Energy_{Engine_2} = 10^{\frac{I_{Engine}}{10}}$$

For the farther engine, the energy is reduced from the initial energy by the attenuation through the jet flow of the closer engine, so that the transmitted energy is given by:

$$T_{Engine_1} = I_{Engine_1} - \alpha(L)$$

Again, the transmitted energy is converted from decibels to a ratio of energies:

$$Transmitted\ Energy_{Engine_2} = 10^{\frac{I_{Engine_1} - \alpha(L)}{10}}$$

The total energy received is the sum of the transmitted energies (note that the subscripts on the initial energies I have been dropped since both engines are assumed to generate the same sound energy):

$$Received\ Energy = 10^{\frac{I - \alpha(L)}{10}} + 10^{\frac{I}{10}}$$

or, converting back to decibels:

$$dB_{received} = 10\log_{10}\left(1 + 10^{-\alpha(L)/10}\right) + I \qquad\qquad \text{Equation 7}$$

Combining equations 6 and 7, then subtracting the un-attenuated two-engine case ($I + 10\ log2$), produces the final general equation for expressing the effect of jet shielding as a difference from the un-attenuated two-engine case:

$$dB_{difference} = 10\log_{10}\left(1 + 10^{-bL/20}\left(\frac{R - \frac{L}{2}}{l}\right)^{-2.3bl^2/10R}\right) - 10\log_{10} 2 \qquad\qquad \text{Equation 8}$$

The variables l and L are defined above in Equation 2 and Equation 3, respectively. The factor of 2.3 in the exponent of equation 8 comes from converting the natural logarithm (ln or log_e) in equation 6 to log_{10}.

For the 767 and DC9, Table 11 shows parameters calculated from the empirical data collected at Wallops using a least squared error algorithm. The parameters in Table 11 are derived from the empirical data; they aren't measured from the physical characteristics of the airplanes. None of these parameters are directly measurable, although the jet flow radius R should approximate to the radius of the exhaust nozzle of the engine and the separation of the engine jet flows should correspond to the physical separation of the engines.

Table 11. DC9 and 767 Empirical Jet Shielding Parameters

Parameter	Physical Meaning	DC9	767
R (feet)	Radius of jet flow	15.1	15.0
d (feet)	Separation of engine jet flows	21.9	39.6
b (dB/ft)	Attenuation	0.90	0.27

The largest difference between a calculated parameter and the corresponding physical parameter is the DC9 jet flow radius. The DC9's JT8D engines have a radius of about 27 inches or a little over 2 feet; this is significantly less than the corresponding calculated jet flow radius of about 15 feet.

For each of these aircraft, Equation 8 goes to zero when L goes to zero, that is, when $R = d$ sin Y, or at Y = arcsine(R/d). Figure 39 and Figure 40 below show the use of the parameters from Table 11 applied to Equation 8, as well as the data used to generate the parameters.

The jet-shielding model can be combined with a simplified ground effects model to produce a lateral attenuation model comparable to SAE-AIR-1751. First the tail-mounted engine installation empirical parameters presented in Table 11 above are modified to accommodate compatibility with SAE-AIR-1751. If the engine installation effect is limited by setting $l = d \sin \theta = d \sin\left(60°\right) = 0.866d$ (from Equation 2), then the engine installation effect is set to zero at angles greater than 60 degrees, as is lateral attenuation in SAE-AIR-1751. Using this constraint on the algorithms produces the set of parameters presented in Table 12. These constrained engine installation parameters produce the small dashed line labeled "Tail-only-EI" shown below in Figure 41. Next, SAE-AIR-1751 is used as a starting point to find a simplified ground effects algorithm. The existing SAE-AIR-1751 lateral attenuation equation is dominated at low angles by the exponential term $-9.9e^{\left(-0.13\theta\right)}$. The other terms in the SAE-AIR-1751 are linear or constant. Because ground effects dominate at low angles, this exponential term can be considered to be the ground effects term. The magnitude of the ground effects at low angles will be determined by the value of the leading constant. Changing this leading constant provides a way to scale the ground effects component. The resulting engine installation and ground effects algorithms can be combined to produce a new lateral attenuation (marked with a light solid line and labeled "Tail-LA" in Figure 41). The SAE-AIR-1751 ground effects term has been scaled to be $-11.26e^{\left(-0.13\theta\right)}$. This scaling, when combined with the tail-mounted engine installation term, provides the same magnitude of lateral attenuation as SAE-AIR-1751.

Table 12. DC9 and 767 Empirical Jet Shielding Parameters, DC9 forced to zero at 60 degrees

Parameter	Physical Meaning	DC9	767
R (feet)	Radius of jet flow	18.7	15.0
d (feet)	Separation of engine jet flows	21.6	39.6
b (dB/ft)	Attenuation	0.54	0.27

The wing-mounted engine installation results of Appendix E are shown in Figure 41 as a dashed-and-dotted line labeled "Wing-only-EI". For the wing-mounted engines, the Wallops engine installation data shows no tendency to continue beyond 20 degrees, so applying SAE-AIR-1751 constraints was not attempted. The combination of the wing-mounted engine installation and the SAE-AIR-1751 ground effects term is shown as the dashed line labeled "Wing-LA". The underlying assumption in these new algorithms is that ground effects are independent of the type and location of the engines. Note that Figure 41, which is based on the simplified jet noise model of this appendix, is similar to Figure 15 in Section 4.7, which is based on the using the first term of the SAE-AIR-1751 equation as the ground effects term.

The combined jet-shielding algorithm and SAE-AIR-1751 ground effects model algorithm produces lateral attenuation results very similar to SAE-AIR-1751 for airplanes with tail-mounted engines. The greatest difference occurs at about 10 degrees where the proposed tail-mounted lateral attenuation is 0.4 dB less than the existing SAE-AIR-1751 algorithm. The differences between the proposed wing-mounted lateral attenuation and SAE-AIR-1751 are greatest at about 20 degrees, where the proposed wing-mounted lateral attenuation is about 2.5 dB less than SAE-AIR-1751.

The following items are known simplifications in the jet shielding model.

- The sound path is actually not straight, but refracted by the impedance mis-match of the ambient conditions and the conditions in the jet flow.

- The geometry is only valid at, or close to, the CPA condition.

- The elevation angle θ has been simplified to represent both the actual elevation angle of the airplane above the ground observer and the angle of the acoustic path through the opposite jet flow.

- The noise source of the jet is assumed to be at the engine's centerline; in reality, the noise source will be
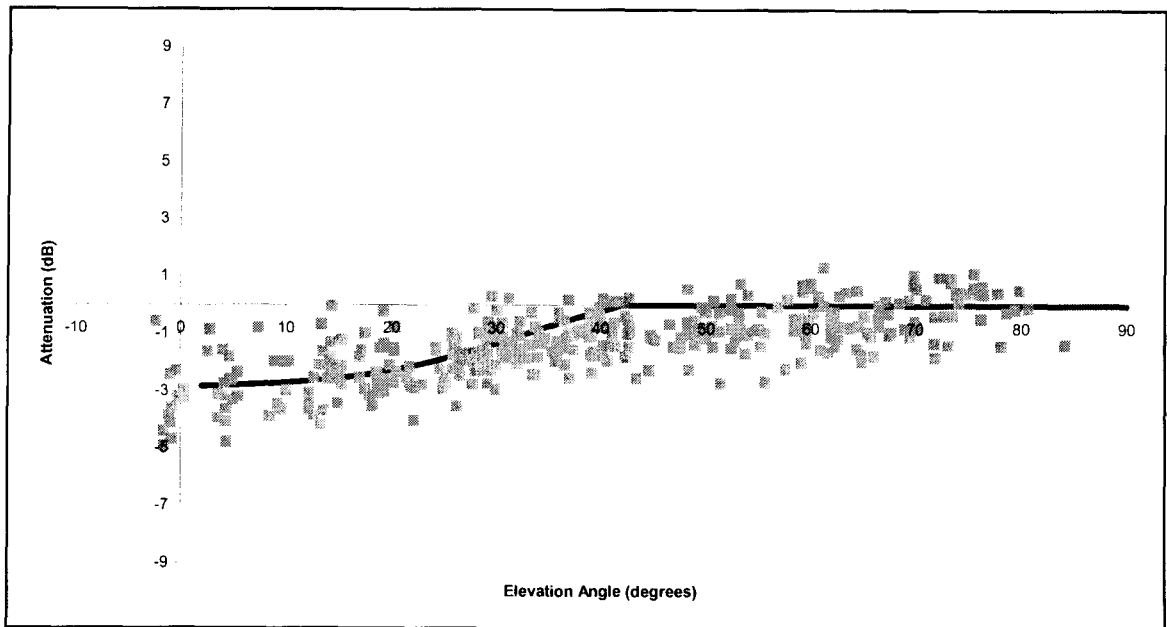
distributed throughout the jet flow radius.

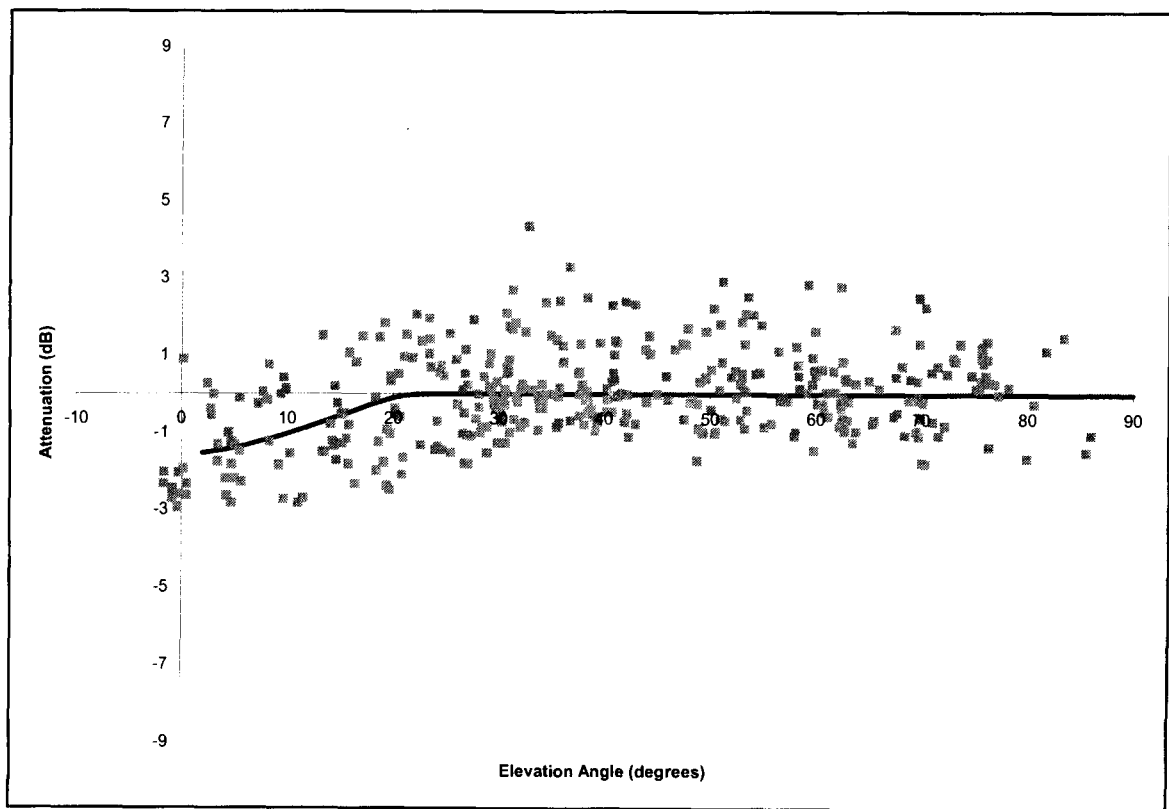Figure 39. DC9 jet shielding model applied to Wallops engine installation data

Figure 40. 767 jet shielding model applied to Wallops engine installation data
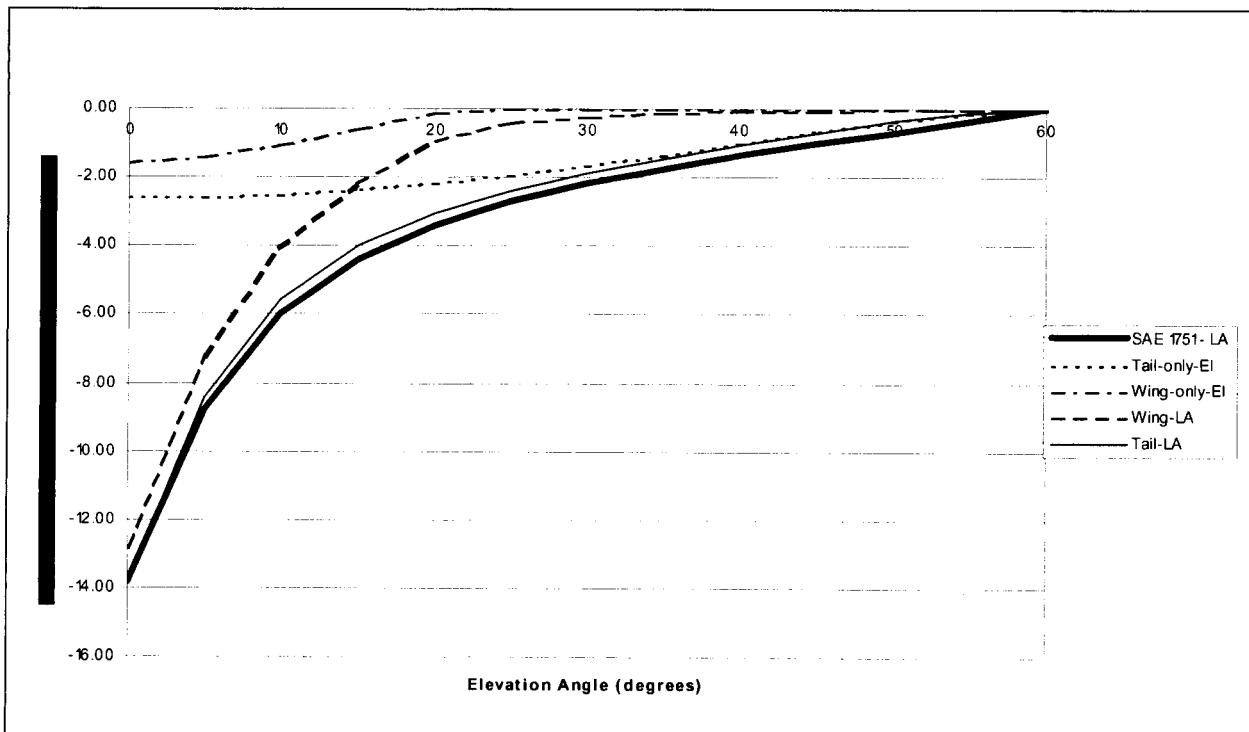
Figure 41. Wing- and tail-mounted lateral attenuation with jet shielding model

Appendix F: List of Acronyms

AIR   Aerospace Information Report

CAA   Civil Aviation Authority

CPA   Closest Point of Approach

dGPS   Differential Global Positioning System

EI   Engine Installation

FAA   Federal Aviation Administration

GE   Ground Effect

LA   Lateral Attenuation

LaRC   Langley Research Center (NASA)

NASA National Aeronautics and Space Administration

NOAA National Oceanic and Atmospheric Administration

SAE   Society of Automotive Engineers

1. REPORT DATE *(DD-MM-YYYY)*	2. REPORT TYPE	3. DATES COVERED *(From - To)*
01- 10 - 2003	Technical Memorandum	October 2000 - May 2003

4. TITLE AND SUBTITLE	5a. CONTRACT NUMBER
Engine Installation Effects of Four Civil Transport Airplanes: Wallops Flight Facility Study	5b. GRANT NUMBER
	5c. PROGRAM ELEMENT NUMBER

6. AUTHOR(S)	5d. PROJECT NUMBER
Gregg G. Fleming, David A. Senzig, David A. McCurdy, Christopher J. Roof, and Amanda S. Rapoza	5e. TASK NUMBER
	5f. WORK UNIT NUMBER
	781-20-11-01

7. PERFORMING ORGANIZATION NAME(S) AND ADDRESS(ES)	8. PERFORMING ORGANIZATION REPORT NUMBER
NASA Langley Research Center,Hampton, VA 23681-2199 U.S. Department of Transportation, John A. Volpe National Transportation Systems Center, Cambridge, MA 02142-1093 Senzig Engineering, 269 Highland Ave., Winchester, MA 01890	L-18305 DTS-34-VX305-LR1

9. SPONSORING/MONITORING AGENCY NAME(S) AND ADDRESS(ES)	10. SPONSOR/MONITOR'S ACRONYM(S)
National Aeronautics and Space Administration Washington, DC 20546-0001	NASA
	11. SPONSOR/MONITOR'S REPORT NUMBER(S)
	NASA/TM-2003-212433

12. DISTRIBUTION/AVAILABILITY STATEMENT
Unclassified - Unlimited
Subject Category - 71
Availability: NASA CASI (301) 621-0390   Distribution: Standard

13. SUPPLEMENTARY NOTES
Fleming, Roof, and Rapoza, U.S. Dept. of Transportation, Cambridge, MA; Senzig, Senzig Engineering, Winchester, MA; McCurdy, Langley Research Center, Hampton, VA. An electronic version can be found at http://techreports.larc.nasa.gov/ltrs/ or http://ntrs.nasa.gov

14. ABSTRACT

The National Aeronautics and Space Administration (NASA), Langley Research Center (LaRC) and the Environmental Measurement and Modeling Division of the United States Department of Transportation's John A. Volpe National Transportation Systems Center (Volpe) conducted a noise measurement study at NASA's Wallops Flight Facility, Virginia, to examine the effects of engine installation on the noise of four civil transport airplanes: a Boeing 767-400, a McDonnell-Douglas DC9, a Dassault Falcon 2000, and a Beechcraft King Air. Acoustic data were collected using a twenty-microphone array configured in a "U" shaped arrangement, with ten microphones mounted on two construction cranes at heights up to 200 feet above ground level, five microphones on each crane, and ten microphones mounted on poles, each at heights of 24 feet above ground level. In addition to detailed acoustic data, time-space-position and meteorological data were also measured. This report presents the results of the study, compares those results with the Society of Automotive Engineers' Aerospace Information Report 1751, and proposes basing new lateral attenuation models on separate engine installation effects and ground effects components.

15. SUBJECT TERMS

noise, aircraft noise, airplane noise, airport noise, engine installation effects, lateral attenuation, INM, Integrated Noise Model, noise prediction, computer noise model, noise contours

16. SECURITY CLASSIFICATION OF:			17. LIMITATION OF ABSTRACT	18. NUMBER OF PAGES	19a. NAME OF RESPONSIBLE PERSON
a. REPORT	b. ABSTRACT	c. THIS PAGE			STI Help Desk (email: help@sti.nasa.gov)
U	U	U	UU	69	19b. TELEPHONE NUMBER *(Include area code)* (301) 621-0390